HHS Public Access

Author manuscript

Neuron. Author manuscript; available in PMC 2021 May 20.

Published in final edited form as:

Neuron. 2020 May 20; 106(4): 649–661.e4. doi:10.1016/j.neuron.2020.02.030.

Muscarinic M1 receptors modulate working memory performance and activity via KCNQ potassium channels in primate prefrontal cortex

Veronica C Galvin[1], **Sheng Tao Yang**[1], **Constantinos D Paspalas**[1], **Yang Yang**[1], **Lu E Jin**[1], **D Datta**[1], **Yury M Morozov**[1], **Taber C Lightbourne**[1], **Adam S Lowet**[1], **Pasko Rakic**[1], **Amy FT Arnsten**[1], **Min Wang**[1,*]

[1]Department of Neuroscience, Yale University School of Medicine, New Haven, CT USA 06520

SUMMARY

Working memory relies on dorsolateral prefrontal cortex (dlPFC), where microcircuits of pyramidal neurons enable persistent firing in the absence of sensory input, maintaining information through recurrent excitation. This activity relies on acetylcholine, though the molecular mechanisms for this dependence are not thoroughly understood. This study investigated the role of muscarinic M1 receptors (M1R) in dlPFC using iontophoresis coupled with single unit recordings from aging monkeys with naturally-occurring cholinergic depletion. We found that M1R stimulation produced an inverted-U dose response on cell firing and behavioral performance when given systemically to aged monkeys. Immunoelectron microscopy localized KCNQ isoforms (Kv7.2, Kv7.3, Kv7.5) on layer III dendrites and spines, similar to M1R. Iontophoretic manipulation of KCNQ channels altered cell firing and reversed the effects of M1R compounds, suggesting KCNQ channels are one mechanism for M1R actions in dlPFC. These results indicate M1R may be an appropriate target to treat cognitive disorders with cholinergic alterations.

eTOC:

Galvin et al. report that muscarinic M1R stimulation is critical for persistent neuronal firing underlying working memory in aged primate dorsolateral prefrontal cortex. Higher M1R

*Corresponding author and Lead Contact: Dr. Min Wang, Dept Neuroscience, Yale University School of Medicine , 333 Cedar Street, New Haven, CT USA 06520 Phone: 1-203-785-5711 min.wang@yale.edu.

Author Contributions

Conceptualization, V.G., A.A. and M.W.
Methodology, V.G., C.P., D.D. and M.W.
Investigation, V.G., S.Y., C.P., Y.Y., L.J., D.D., Y.M., T.L., A.L., and M.W.
Writing – Original Draft, V.G., A.A. and M.W.
Writing – Review & Editing, V.G., S.Y., C.P., Y.Y., L.J., D.D., Y.M., T.L., A.L., P.R., A.A. and M.W.
Funding Acquisition, M.W., A.A., Y.Y.
Resources, A.A. and M.W.
Supervision, P.R., A.A. and M.W.

Declaration of Interests

The authors declare no competing interests.

stimulation produced an inverted-U effect on neuronal firing and behavioral performance. M1R beneficial actions involved KCNQ channel closure, which may interact with M1R on spines.

Keywords

Acetylcholine; muscarinic; M1; cholinergic; prefrontal cortex; dorsolateral prefrontal cortex; working memory; aging; schizophrenia; KCNQ

INTRODUCTION

The prefrontal cortex (PFC) is the most newly evolved cortical region, and has shown great expansion across primate evolution (Elston et al., 2006). These newly evolved circuits are critical for high order cognition, executive functioning, top-down regulation of emotion and behavior, attention, and working memory (WM). PFC dysfunction is cardinal to many psychiatric disorders such as schizophrenia (Barch and Smith, 2008; Cannon et al., 2005), as well as to age-related cognitive decline and cognitive devastation in Alzheimer's disease (AD) (Bussiere et al., 2003a; Bussiere et al., 2003b; Dumitriu et al., 2010). Evidence suggests that acetylcholine (ACh) has critical influences on PFC function, with relevance to the etiology and treatment of cognitive disorders.

ACh axons strongly innervate the PFC via projections from the basal forebrain (Mesulam et al., 1983). These ACh projections to PFC play a role in many cognitive processes such as attentional gating and signal detection (Berry et al., 2014; Gritton et al., 2016; Parikh et al., 2007), abstract rule representation (Everling and DeSouza, 2005; Wallis et al., 2001), inhibiting inappropriate behaviors (Condy et al., 2007) as well as WM (Croxson et al., 2011). Evidence points to a particularly essential role for ACh in WM functions of the dorsolateral PFC (dlPFC), as cholinergic depletion to this area caused significant WM impairments equitable to tissue ablation (Croxson et al., 2011; Goldman et al., 1971). Reductions in cholinergic signaling in PFC may also contribute to cognitive disorders. Loss of cholinergic receptors has been reported in PFC of patients with schizophrenia, and the high rates of smoking in these patients are thought to be a form of self-medication (Dean et al., 2002; Guan et al., 1999; Hughes et al., 1986). Cholinergic depletion in PFC is consistently reported in aging (Mesulam et al., 1987) and AD (Grothe et al., 2012; Morrison and Hof, 2007). It has long been appreciated that AD is associated with a loss of basal forebrain cholinergic neurons (Bowen et al., 1976; Grothe et al., 2013; Grothe et al., 2012), with evidence of a correlation between degree of dysfunction and loss of ACh markers (Perry et al., 1981). Indeed, current cholinergic treatments for AD arose from studies in monkeys showing that muscarinic receptor antagonists could induce profound impairments in WM function, while agents that enhanced cholinergic signaling could improve WM in aged monkeys with naturally-occurring loss of cholinergic inputs (Bartus and Dean, 1988; Bartus et al., 1982; Wenk et al., 1989).

WM, or the ability to hold information "in mind", relies on recurrent microcircuits within dlPFC. Electrophysiological recordings from non-human primates identified neurons within dlPFC that show persistent firing over the delay period in a WM task maintaining information in temporary storage until needed to guide thought or behavior (Funahashi et al.,

1989). These “Delay cells” have been especially well characterized for spatial working memory, with Delay cells firing for particular “preferred” spatial locations and not for other locations in the visual field (Figure 1D). The circuitry underlying this persistent delay activity was uncovered by Goldman-Rakic and colleagues, residing in deep layer III of dlPFC, where pyramidal neurons show extensive horizontal projections to support recurrent excitation between similarly tuned cells across delay periods (Goldman-Rakic, 1995; Gonzalez-Burgos et al., 2000).

These excitatory synaptic connections underlying persistent delay activity rely on NMDA receptor (NMDAR) activation, particularly those containing NR2B subunits (Wang et al., 2013). Recent work has uncovered a unique permissive role for ACh in these NMDAR circuits during working memory delays. In classic excitatory glutamatergic synapses, AMPA receptor (AMPAR) activation provides the critical membrane depolarization needed to eject magnesium and allow NMDAR activation. However, in dlPFC Delay cells, AMPAR play a surprisingly minimal role, and ACh provides this critical depolarization step via activation of nicotinic α7 receptors expressed within the postsynaptic density (PSD) on dendritic spines (Yang et al., 2013). As ACh is released during waking but not deep sleep, cholinergic mechanisms may provide a state change that permits dlPFC network engagement (Jones, 1993).

Muscarinic M1 receptors (M1Rs) are also expressed postsynaptically on spines in dlPFC (Mrzljak et al., 1993), though their role in these circuits has only recently begun to be investigated. Recent work by the Everling group assessed the effects of applying M1R selective antagonists and agonists to cells in dlPFC while young rhesus monkeys performed a cognitive control task with a WM component. They found activity during the delay period was consistently reduced following application of an M1R antagonist (Major et al., 2015, 2018), but report mixed results following application of an M1R selective agonist, either exciting or suppressing activity, suggesting an inverted-U for M1R actions in dlPFC (Vijayraghavan et al., 2018). As these experiments were performed in young adult, cognitively healthy primates, the results suggest there may be ceiling effects for M1R enhancing actions in young monkeys with high endogenous cholinergic activity in PFC. In contrast, aged monkeys with naturally-occurring loss of ACh, reduced persistent firing (Wang et al., 2011) and impaired WM (Rapp and Amaral, 1989), may offer an important opportunity to explore the molecular mechanisms underlying potential beneficial actions at M1R.

M1Rs are metabotropic receptors and can indirectly influence the synaptic membrane potential via G-protein signaling cascades to regulate the open state of downstream ion channels (Thiele, 2013). M1R may have opposing actions on excitability through its effects on the KCNQ (KCNQ1–5; Kv7.1–7.5) family of potassium channels. KCNQ2, KCNQ3, and KCNQ5 are found in brain, where they can form heteromeric (KCNQ2/3, KCNQ3/5) as well as homomeric channels (Delmas and Brown, 2005). M1R can excite neural membranes by closing KCNQ channels via PIP2 signaling (Suh and Hille, 2002); thus, KCNQ channels are often referred to as “M channels”. This change in channel conductance occurs fast, with complete closure within 5–16s of M1R stimulation (Suh and Hille, 2002; Suh et al., 2004). However, M1Rs can also hyperpolarize the membrane through downstream PKC-cAMP-

PKA signaling mechanisms that increase the open state of KCNQ2 channels (Iyengar, 1993). Thus, M1R-Gq activation can potentially influence WM circuits through two parallel but opposing signaling pathways (summarized in Figure 1E and 1F).

The current study investigated the effects of manipulating M1Rs and KCNQ channels in dlPFC in aged primates performing a WM task, using iontophoretic application of compounds directly near recorded neurons (Figure 1B). We validated prior reports of the subcellular location of M1Rs on spines in dlPFC using immunoelectron microscopy (immunoEM), and found that low dose stimulation of M1R enhanced Delay cell firing, while M1R blockade reduced Delay cell firing. We also performed the first immunoelectron microscopic (immunoEM) localization of KCNQ channels in primate dlPFC, and found blockade or stimulation of KCNQ channels could reverse the reduction or enhancement of Delay cell firing following M1R blockade or stimulation. Finally, we characterized the effects of systemic application of a novel M1R-selective positive allosteric modulator (PAM) on WM performance in aged primates, finding potential for low dose, therapeutic actions.

RESULTS

M1R localization and physiology in primate dlPFC

Muscarinic M1R have previously been localized to layer III spines in rhesus monkey dlPFC (Mrzljak et al., 1993), a finding that we have replicated in the current study (Figure 2A-C and S1). M1R were seen near the PSD (Figure 2A-B) and at extrasynaptic (Figure 2C) locations. We also found M1R localization near the plasma membrane on dendrites (Figure 2D), including dendrites with an interneuron-like profile, receiving multiple, glutamate-like synapses (Figure 2E). In addition, we found frequent M1R expression on astrocytes (Figure S2A-B), including astrocytic leaflets ensheathing axospinous asymmetric synapses (Figure S2C).

M1R blockade reduces delay-related firing and spatial tuning

We recorded Delay cells (Figure 1D) from the dlPFC (Figures 1C) of one middle-aged (age 16, male) and two aged monkeys (age 20, male and age 21, female) performing the oculomotor delayed response (ODR) task (Figure 1A), while applying compounds that block vs. stimulate M1R. Pharmacological agents were applied directly onto recorded neurons using iontophoresis (Figure 1B); levels were sufficient to alter the activity of a small number of neurons but inadequate to alter behavioral performance. As middle-aged and aging monkeys have naturally-occurring depletion of ACh (Wenk et al., 1989), these animals provide the opportunity to enhance as well as block M1R actions, and thus investigate the full spectrum of cholinergic M1R actions in the primate dlPFC.

The first experiment examined the effects of the general muscarinic antagonist, scopolamine, on dlPFC Delay cells. Consistent with previous findings (Major et al., 2015), scopolamine significantly reduced dlPFC Delay cell firing, reducing neuronal activity for both the preferred and nonpreferred directions (Figure S3). Overall, scopolamine significantly reduced the spatial tuning of Delay cells, eroding their representations of visual space in working memory as measured by d’ (Figure S3D).

The second set of experiments specifically investigated the role of endogenous cholinergic stimulation of M1Rs by examining the effects of selective M1R antagonists on dlPFC Delay cell firing. The M1R selective antagonist telenzepine (telen) was tested at a range of doses (10nA-40nA). As shown in Figure 3A, iontophoretic application of telen significantly reduced activity during the delay period for the neuron's preferred direction, reducing representation of visual space (Figure 3A: preferred direction: control vs telen, $t(16)=8.36$, $p<0.0001$; non-preferred direction: control vs telen, $t(16)=1.432$, $p=0.171$, unpaired t test). Delay–related activity was restored toward control levels when the drug was no longer applied (preferred direction: recovery vs telen, $t(18)=6.81$, $p<0.0001$; recovery vs control, $t(16)=1.537$, $p=0.143$, unpaired t test). At a population level (n=29), telen reduced delay-related firing in 27 out of 29 Delay cells, and increased delay-related firing in 2 out of 29 Delay cells. Overall, telen reduced delay firing for both the neurons' preferred direction and non-preferred direction. Further analysis indicated that telen produced a greater reduction for the preferred directions (Figure 3B; R-two-way ANOVA, $F_{direction\times drug}(1,28)=19.59$, $p=0.0002$; Sidak's multiple comparisons: preferred direction, $p<0.0001$ and non-preferred direction, $p=0.0427$) and telen significantly reduced the d' measure of spatial tuning in 23 out of 29 Delay cells (Figure 3B, control vs telen, $t(28)=4.164$, $p=0.0003$, two-tailed paired t test).

The effects of telen were replicated with another M1R selective antagonist, pirenzepine (piren). A single neuron example illustrates that piren significantly reduced delay-related activity (Figure S4). Of the 14 Delay cells tested with piren, 11 decreased delay-related firing after piren application. Overall, piren significantly reduced delay-related firing for the neurons' preferred direction, but not for the nonpreferred direction. As a result piren produced a greater reduction for the preferred directions (Figure 3C, R-two-way ANOVA, $F_{direction\times drug}(1,13)=12.55$, $p=0.003$; Sidak's multiple comparisons: preferred direction, $p<0.0001$ and non-preferred direction, $p=0.0524$), and significantly reduced the d' measure of spatial tuning (Figure 3C, control vs piren, $t(13)=2.875$, $p=0.013$, two-tailed paired t test).

In summary, endogenous ACh actions at M1Rs are important for spatial working memory, as both selective M1R antagonists reduced delay-related firing and spatial tuning, weakening the representation of visuospace.

Low dose M1R stimulation enhances Delay cell firing and spatial tuning

We next examined the effect of two M1R agonists, cevimeline (cevi) and xanomeline (xano) on Delay cell firing. Iontophoresis of a low dose (10–20nA) of xano increased delay firing and enhanced spatial tuning. As shown in Figure 4A, xano at a dose of 20nA significantly increased delay firing for both the preferred (control vs xano, $t(22)=2.543$, $p=0.018$, unpaired t test) and nonpreferred directions (control vs xano, $t(22)=2.666$, $p=0.014$, unpaired t test). Overall, xano significantly enhanced spatial tuning for this Delay cell (control d'=2.46, xano d'=3.18). Delay-related activity was reduced toward control levels when the drug was no longer applied (preferred direction: recovery vs xano, $t(25)=2.2838$, $p=0.009$; recovery vs control, $t(25)=0.106$, $p=0.916$, unpaired t test).

Similar results were observed for the entire population of Delay cells tested (Figure 4B, n=11), where xano increased delay-related firing for both the preferred direction and the

nonpreferred directions. The stronger drug actions on firing for the preferred direction (Figure 4B, R-two-way ANOVA, $F_{direction\times drug}(1,10)=16.33$, p=0.0024; Sidak's multiple comparisons: preferred direction, p<0.0001 and non-preferred direction, p=0.1855) led to a significant increase in spatial tuning as measured by d' (Figure 4B, control vs xano, t(10)=3.801, p=0.004), two-tailed paired t test).

To confirm that the enhancing effects of xano were due to actions at M1Rs, we co-applied the M1R antagonist, telen, with xano. We found that co-iontophoresis of telen with xano blocked the enhancing effects of xano alone. This experiment purposefully utilized a low dose of telen (10nA) that had no significant effect on its own, as shown in Figures 4D and S5, and xano was unable to enhance delay-related firing in the presence of telen (Figure 4D; preferred direction: control vs telen, t(14)=0.566, p=0.58; control vs. telen+xano, t(14)=0.272, p=0.78; nonpreferred direction: control vs telen t(14)=0.53, p=0.60; control vs telen+xano, t(14)=0.693, p=0.49, unpaired t test). These results are consistent with xano acting at M1R.

Low doses of the M1R agonist cevi had similar effects as xano, shown in a single neuron example (Figure S6) and at the population level (n=14, Figure 4C). Iontophoresis of low doses of cevi increased Delay cell firing for both the preferred direction, and for the nonpreferred direction. Similar to xano, the increased firing for the neurons' preferred direction with low dose cevi predominated (Figure 4C, R-two-way ANOVA, $F_{direction\times drug}(1,13)=8.369$, p=0.0126; Sidak's multiple comparisons: preferred direction, p<0.0001 and non-preferred direction, p=0.0046), enhancing spatial tuning (Figure 4C, control vs cevi, t(13)=2.873, p=0.013, two-tailed paired t test).

We also tested a novel positive allosteric modulator (PAM), VU0357017 (VU035), on Delay cell firing. Iontophoresis of a low dose (10–20nA) of VU035 produced a dose-related enhancement of Delay cell firing. A single neuron example (Figure 4E) shows that VU035 at 10nA tended to enhance firing, while the 20nA dose significantly increased delay firing for the neuron's preferred but not nonpreferred direction. This same enhancement by VU035 was evident at the population level, with significance for the preferred direction, but not for the nonpreferred direction. As a result, low doses of VU035 significantly improved the d' measure of spatial tuning (Figure 4F; R-two-way ANOVA, $F_{direction\times drug}(1, 23)=16.94$, p=0.0004; Sidak's multiple comparisons: preferred direction, p<0.0001 and non-preferred direction, p=0.6246; d': control vs VU035, t(23)=2.727, p=0.01, two-tailed paired t test).

In summary, low doses of an M1R PAM and two M1R agonists all had the same beneficial actions of preferentially increasing firing for the neurons' preferred direction, thus enhancing visuospatial representation.

Higher dose of M1R produces mixed effects on delay-related firing and behavior

Some neurons were sufficiently stable to assess additional, higher doses (30–40nA) of the M1R agonists or the M1R PAM. In contrast to the consistent enhancement produced by lower doses (10–20nA), the application of higher doses (30–40nA) had mixed effects on delay firing. Some neurons showed a linear, dose-related increase in delay firing with increasing dose, while others showed an inverted U dose response and decreased firing. An

example of an individual neuron with a dose-related increase in firing is shown in Figures 5A and S7A. A low dose of VU035 or xano (20nA) increased delay firing for the preferred direction and higher dose application of VU035 or xano at 40nA further increased delay firing. In contrast, an example of an individual neuron with an inverted U dose response is shown in Figures 5B and S7B. VU035 at 20nA or xano at 15nA significantly increased delay firing for the preferred but subsequent application of VU035 at 40nA or xano at 30nA decreased delay firing.

This mixed, inverted-U effect of M1R stimulation was evident at the population level, with 5 of 7 neurons showing decreased firing at higher doses of xano (Figure S7C) to levels not significantly different from baseline ($p=0.578$). A similar pattern was seen in cevi, where 7 of 9 Delay cells decreased firing at higher doses of cevi (Figure S7D), reducing activity to levels not significantly different from control ($p=0.0977$). Higher doses of VU035 also reduced spatial tuning, primarily by decreasing firing for the preferred direction (Figure 5B). At the population level (Figure 5C), this was a consistent effect, with 7 of 10 neurons showing significantly reduced delay-related firing at higher doses of VU035, to activity levels not significantly different from control ($p=0.3223$).

We found similar, inverted-U dose response effects of the M1R PAM VU0453595 (Ghoshal et al., 2016) on behavioral performance of a spatial working memory task in a Wisconsin General Testing Apparatus when seven aged rhesus monkeys were given this compound systemically (i.m. 60 min before testing). We tested a wide range of doses (0.001ug/kg – 1.0ug/kg) and found a similar inverted-U dose-response as the electrophysiological experiments, with improvement in behavioral performance at lower doses (VEH vs. 0.001 ug/kg, $p=0.0227$, Dunnett's multiple comparisons test; VEH vs. 0.01 ug/kg, $p=0.0173$, Dunnett's multiple comparisons test) but no change or inconsistent enhancement at higher doses (Figure 5D, $F(2.16,12.96) = 3.166$, $p=0.0731$ repeated measures ANOVA; significant quadratic fit $F(1,6) = 1.434$, $p=0.035$). As the peak dose for each animal was slightly variable within the lower doses, we compared the best dose for each animal to their baseline vehicle response and found a significant improving effect of VU0453595 on working memory performance (Figure 5D, "best dose" vs. VEH; $p=0.0013$, two tailed paired samples t test).

These effects support an inverted-U dose response for M1R activation on behavior and delayrelated firing, where low doses enhance neuronal representations of visuospace and working memory performance, while higher doses erode this enhancement. This is consistent with other recent experiments investigating M1R actions in PFC in young adult monkeys, where the suppressive effects of M1R over-stimulation predominate at higher doses (Vijayraghavan et al., 2018).

KCNQ channel actions in primate dlPFC

As M1R enhancing effects on delay-related firing may involve closure of KCNQ channels, we characterized the localization and physiological contributions of KCNQ channels in primate dlPFC.

KCNQ2, KCNQ3, and KCNQ5 channel isoforms are localized on layer III dlPFC spines

The current study performed the first localization of KCNQ channels (KCNQ2, KCNQ3, and KCNQ5) in layer III of the primate dlPFC. As a complete characterization of KCNQ channel localization was beyond the scope of the current study, we focused on their potential location on spines and dendrites, where M1R are localized in primate dlPFC. We found that all three isoforms were localized on spines and dendrites in layer III dlPFC. KCNQ5 were seen in spines, often near the PSD (Figures 6A-C), as well as on dendrites (e.g. Figure 6C). Both KCNQ3 and KCNQ2 were seen at peri- and extra-synaptic locations on spines (Figures 6D-E and 6G-H), as well as having prominent localization on dendrites (Figures 6F and 6I). As with M1R, there were also examples of KCNQ3 on dendrites with interneuron-like characteristics (Figure S8). Thus, KCNQ channels were in similar locations to those of M1R in dendritic trees and spines.

Blocking KCNQ channels strengthens, while opening KCNQ channels suppresses, delayrelated firing

We first tested the effects of blocking KCNQ channels on Delay cell firing. Iontophoresis of a low dose (10–25nA) of the KCNQ channel blocker, XE991, enhanced delay-related firing (single cell example shown in Figure 7A; control vs XE991: preferred direction, $t(17)=3.692$, $p=0.002$, nonpreferred direction, $t(13)=1.617$, $p=0.13$, unpaired t test). At the population level (n=25), low doses of XE991 increased firing for both the preferred direction, and the nonpreferred direction. This enhancement was greater for the preferred direction (Figure 7B, R-two-way ANOVA, $F_{directionxdrug}(1, 24)=4.71$, $p=0.0234$; Sidak's multiple comparisons: preferred direction, $p=0.0022$ and non-preferred direction, $p=0.7759$), causing low doses of XE991 to significantly enhance the spatial tuning measure d' (Figure 7B, control vs. XE991, $t(24)=3.095$, $p=0.005$, two-tailed paired t test).

We next tested the effects of increasing the open state of KCNQ channels with retigabine, a PAM with high affinity for KCNQ3 and KCNQ2/3, but lower affinity for KCNQ5, and effectively no affinity for the cardiac channel, KCNQ1 (Gunthorpe et al., 2012). Retigabine caused a reduction in Delay cell firing for the preferred direction in a dose dependent manner (single cell example shown in Figure 7C; preferred direction: one-way ANOVA, $F(2,24)=6.149$, $p=0.007$; Tukey's multiple comparisons: control vs retigabine@25nA, $p>0.05$ and control vs retigabine@50nA, $p<0.01$). This dose dependent reduction was consistent at the population level (Figure 7D, preferred direction: R-one-way ANOVA, $F(1.734, 15.6)=14.94$, $p=0.0004$; Tukey's multiple comparisons: control vs retigabine@25nA, $p=0.69$ and control vs retigabine@50nA, $p=0.0038$). Iontophoresis of retigabine at 25nA produced non-significant reductions in delay firing and spatial tuning (Figure 7D, $t(9)=2.019$, $p=0.074$), while retigabine at 50nA significantly reduced both delay related firing and spatial tuning ($t(9)=4.886$, $p=0.0009$). The higher doses needed with retigabine may be related to its preference for KCNQ3, with higher doses needed to engage KCNQ2 and KCNQ5.

KCNQ channel interactions with M1R

KCNQ opening blocks the enhancing effects of M1R stimulation

If the enhancing effects of M1R stimulation are mediated through closure of KCNQ channels, these beneficial effects should be blocked by increasing the open state of KCNQ channels. Indeed, as illustrated in Figure 8A, a low dose of the M1R PAM VU035 enhanced Delay cell firing, and this enhancement was reversed by subsequent co-application of VU035 with retigabine at 25nA (Figure 8A; preferred direction: one-way ANOVA, $F(2,29)=5.296$, $p=0.011$; Tukey's multiple comparisons: control vs VU035, $p=0.001$; control vs VU035+retigabine, $p=0.804$; VU035 vs VU035+retigabine, $p=0.02$). This reversal by retigabine (25nA) was significant in 6 of 6 Delay cells tested both for their firing rate (Figure 8B; preferred direction: R-one-way ANOVA, $F(1.112, 5.559)=17.2$, $p=0.0065$; Tukey's multiple comparisons: control vs VU035, $p=0.0183$; VU035 vs VU035+retigabine, $p=0.0292$) and for their spatial tuning (Figure 8C; R-one-way ANOVA, $F(2, 10)=4.778$, $p=0.035$; Tukey's multiple comparisons: control vs VU035, $p=0.0835$; VU035 vs VU035+retigabine, $p=0.0403$).

KCNQ blockade prevents the deleterious effects of M1R antagonism

We next performed the converse experiment, and tested whether the loss of firing with M1R blockade could be reversed by blockade of KCNQ channels with XE991. Iontophoresis of the M1R antagonist, telen, produced the expected reduction in delay-related firing, and subsequent co-application of XE991 with telen restored delay-related firing (Figure 8D, preferred direction: one-way ANOVA, $F(2,35)=8.351$, $p=0.0011$; Tukey's multiple comparisons: control vs telen, $p=0.003$; telen vs telen+XE991, $p=0.0063$). This recovery was significant at the population level, where 7 out of 7 Delay cells tested showed firing levels significantly increase with telen+XE991 compared to telen alone (Figure 8E; preferred direction: R-one-way ANOVA, $F(1.597, 9.584)=7.207$, $p=0.0155$; Tukey's multiple comparisons: control vs telen, $p=0.0523$; telen vs telen+XE991, $p=0.011$). Iontophoresis of telen significantly reduced spatial tuning, but subsequent co-application of telen+XE991 rescued spatial tuning toward baseline levels (Figure 8F; R-one-way ANOVA, $F(1.949, 11.7)=5.177$, $p=0.0251$; Tukey's multiple comparisons: control vs telen, $p=0.0191$; telen vs telen+XE991, $p=0.2072$).

Taken together, these findings support the hypothesis that M1R stimulation enhances Delay cell firing at least in part through closure of KCNQ channels in primate dlPFC.

DISCUSSION

Summary

Here we show a mechanism for M1R modulation of PFC neuronal activity via control of KCNQ potassium channel open state. We report that both M1R and KCNQ channels are localized on dendrites and spines in layer III of monkey dlPFC, the layer that contains the recurrent excitatory microcircuits needed for persistent firing. We found that local application of compounds that block M1R reduce Delay cell firing, and application of compounds that stimulate M1R produce a quite narrow, inverted-U dose response in aging macaques, where low-dose M1R agonists or PAMs enhanced delay-related firing, but higher

doses reduced delay-related firing. This inverted-U dose response is consistent with the effects of other neuromodulatory systems on Delay cell activity in PFC such as dopamine (Vijayraghavan et al., 2007), norepinephrine (Wang et al., 2007), and cholinergic actions at nicotinic receptors (Yang et al., 2013). A variety of mechanisms can erode responses at high doses, e.g. by activating negative feedback mechanisms or producing nonspecific excitation, or by engaging additional cell types such as GABAergic interneurons (Arnsten and Wang, 2016). These data highlight the sensitivity of dlPFC circuits compared to V1 for example, where nicotinic agonists show a linear dose response within individual neurons (Disney et al., 2007).

These findings of M1R-induced reduction in neuronal firing with high doses of receptor stimulation or receptor blockade are consistent with previous reports from young adult monkeys performing a related task (Major et al., 2015; Vijayraghavan et al., 2018). The most recent study by the Everling group reported mixed results with low dose M1R PAM stimulation, where 49% of neurons were inhibited following low dose application and 31% significantly excited, whereas here we report consistent enhancement of delay firing in the same dose range. We interpret these differences to be explained by our use of aging monkeys with naturally-occurring cholinergic loss (Wenk et al., 1989), reduced Delay cell firing (Wang et al., 2011), and impaired working memory (Rapp and Amaral, 1989), which allowed us to fully explore the beneficial effects of M1R stimulation without the ceiling effects inherent in studies of young monkeys. Thus, we were able to observe an enhancing effect of low dose M1R stimulation on Delay cell firing, and could explore downstream mechanisms to explain this enhancement which we show here is at least in part via actions on KCNQ “M” channels. It is also possible the differences in reported results of M1R stimulation could be due to other factors such as task differences. The task used by Vijayraghavan et al. is similarly an oculomotor task with a delay component, but with interleaved pro- and antisacade trials indicated by a color change of the fixation point with only two possible saccade locations instead of a presented cue. It is possible the requirement of long term memory for which direction the cue color indicates versus our visual guided cue working memory task could contribute to these differences, though this seems unlikely given the task similarity. Our parallel behavioral study also found an inverted-U dose response following systemic administration of an M1R PAM, where very low doses could improve the spatial working memory performance of aged monkeys, further supporting age as a possible explanation for reported differences with M1R stimulation. Our data suggest the pursuit of M1R stimulation for therapeutics may be best for aging populations or patients with otherwise reduced cholinergic tone.

Potential mechanisms of action—Our physiological findings support a functional interaction between the enhancing effects of low dose M1R stimulation and the closure of KCNQ “M”-channels in dlPFC. The beneficial effects of increasing M1R stimulation with low doses of VU0357017 were reversed by increasing the open state of KCNQ channels with a dose of retigabine that had no effect on delay firing alone. Conversely, the suppression of delay activity with the M1R antagonist telenzepine was reversed by the KCNQ channel blocker, XE991. As both M1R and KCNQ channels are expressed on the plasma membrane of spines and dendrites in layer III dlPFC, the physiological data support

the hypothesis that low dose M1R stimulation enhances Delay cell firing by closing KCNQ channels via the fast hydrolysis of PIP2, where *in vitro* experiments show complete reduction of M-current within 5–16s of M1R stimulation (Suh and Hille, 2002; Suh et al., 2004). While activation of metabotropic M1R can initiate a cascade of second messenger actions (e.g. Figure 1F), our data are consistent with the known, powerful effects of M1R in closing KCNQ “M” channels.

The mechanisms underlying the reduced firing at higher doses of M1R stimulation are likely complex, and were not addressed in the current study. Vijayraghavan et al (2018) suggest they may involve off-target drug effects, e.g. on M2R, but it is also possible that neurons reduced firing through additional M1R-mediated actions. For example, the current finding of M1R and KCNQ3 on interneuron-like dendrites suggests that higher dose M1R stimulation may reduce Delay cell firing by directly exciting GABA inhibition of pyramidal cells, e.g. by closing KCNQ3 at these sites. Higher dose stimulation may also drive indirect glutamatergic stimulation of PV+ interneurons, leading to a reduction in circuit firing (Tikhonova et al., 2018). Higher levels of M1R stimulation may also reduce firing by increasing Gq-PKC-AC-cAMP signaling within pyramidal cells, as illustrated in Figure 1F. The KCNQ2 isoform is sensitive to cAMP-PKA signaling, where KCNQ2 conductance is *increased* by PKA phosphorylation (Delmas and Brown, 2005; Schroeder et al., 1998), leading to a reduction in neuronal firing (Arnsten et al., 2019). As Gq-Ca2+-PKC signaling can increase the production of cAMP, this signaling cascade may also drive PKA signaling to open KCNQ2 channels and reduce Delay cell firing. This is consistent with previous data showing that PKC activation leads to reduced Delay cell firing and impaired working memory in young adult monkeys (Birnbaum et al., 2004). Thus, M1R activation may differentially regulate KCNQ channels depending on their subunit composition and location. An inverted-U dose-response may be inherent within the M1R-Gq signaling cascade, with low levels closing all KCNQ channel isoforms, and the higher levels of M1R stimulation leading to an increased opening of KCNQ2 to produce negative feedback and prevent seizures. This is an important, but complex area for future research.

Relevance to cognitive dysfunction and psychiatric disease—Cholinergic actions at muscarinic receptors are important for working memory functions, and for higher cognitive disorders with pronounced PFC impairments. As It has long been appreciated that systemic administration of general muscarinic antagonists such as scopolamine impair working memory performance in monkeys and humans (Bartus and Dean, 1988; Green et al., 2005) mimicking deficits seen in aging monkeys and humans (Bartus et al., 1982). These pharmacological data are consistent with the impairments in working memory induced by cholinergic depletion in monkey PFC (Croxson et al., 2011), and with the current data showing reduced Delay cell firing following iontophoresis of scopolamine. Our data suggest these deficits in working memory arise at least in part from actions at M1Rs in PFC, as we found significant reductions in delay-related firing following selective M1R blockade.

Accumulating evidence also points to a key role for ACh in the cognitive deficits associated with aging in AD, where patients show reduced cholinergic innervation of cortex and paralimbic regions, reduced choline acetyltransferase (ChAT) activity, and atrophy of cholinergic nuclei in the BF, with the degree of BF loss correlating with cognitive

dysfunction (Geula and Mesulam, 1989; Gibson and Peterson, 1981; Gibson et al., 1981; Grothe et al., 2012; Mesulam et al., 1986). These data led to the development of currently available treatments for AD targeting the inhibition of acetylcholinesterase to prolong ACh actions (Galimberti and Scarpini, 2016). Both our physiological results and behavioral data indicate that low doses of an M1R positive allosteric modulator may be a useful treatment option for cognitive deficits in these patients prior to degeneration of cortical pyramidal cells in later stage disease. However, the data also caution that doses must be kept very low, as beneficial effects are lost at higher doses.

Cholinergic dysfunction is also evident in schizophrenia, and cholinergic receptors have been a recent target for therapeutic drug development in this disorder. Schizophrenic patients have much higher smoking rates than the general population, thought to be a potential method of self-medication (Hughes et al., 1986), and systemic anticholinergic agents worsen both positive and cognitive symptoms in otherwise unmedicated subjects (Veselinovic et al., 2015). Postmortem studies of brains from patients with schizophrenia have reported reductions in nicotinic α7 receptor protein, M1R protein, and M1R mRNA levels in PFC (Dean et al., 2002; Guan et al., 1999). Nicotinic a7 receptor agonists have been a recent target for therapeutic potential, though clinical trials reported mixed results, likely due to a narrow therapeutic window (Freedman et al., 2008; Keefe et al., 2015; Yang et al., 2013). It is possible that low dose M1R agonists or PAMs may be a more effective strategy, and the M1R selective agonist xanomeline is currently being tested in clinical trials by Karuna Therapeutics under the name KarXT, where significant improvement was recently reported in a Phase 2 trial.

KCNQ channels are also associated with neuropsychiatric disorders, especially with epilepsy and overall intellectual disability. For example, benign neonatal familial convulsions (BNFC) are caused by a mutation in KCNQ2 that prevents PKA increasing the KCNQ2 open state (Brown, 2008). Retigabine was developed as an anti-epileptic agent, but had side effects including confusion and memory impairment, and has been discontinued from use (Clark et al., 2015). There are also studies suggesting an association between KCNQ2 and KCNQ3 with bipolar disorder, including lower expression of KCNQ3 in post-mortem PFC (Borsotto et al., 2007; Kaminsky et al., 2015). KCNQ2, KCNQ3 and KCNQ5 have all been associated with intellectual disability and social deficits found in autism spectrum disorders independent from or co-morbid with epileptic symptoms (Kim et al., 2019; Lehman et al., 2017; Miceli et al., 2015). Our findings suggest some of these deficits in cognitive functioning may be due to the role of KCNQ channels in regulating dynamic network connectivity of PFC circuits via expression on glutamatergic spines, and that use of retigabine for neuropsychiatric disorders may be problematic given its suppression of Delay cell firing.

As KCNQ channels are widely expressed in the central nervous system and, depending on location and isoform composition, have multiple effects on neuronal excitability, our data suggest M1Rs may be a more selective route for enhancing PFC physiology. The current results provide a mechanism for M1R contributions to cholinergic actions in dlPFC, and show that low dose stimulation of these receptors could be a selective means of boosting PFC circuits under conditions of reduced cholinergic tone.

STAR Methods

LEAD CONTACT AND MATERIALS AVAILABILITY

Further information and requests for resources and reagents should be directed to and will be fulfilled by the Lead Contact, Min Wang (min.wang@yale.edu).

This study did not generate any new unique reagents.

EXPERIMENTAL MODEL AND SUBJECT DETAILS

The electrophysiology experiments were performed with one middle-aged (age 16, male) and two aged (age 20, male and 21, female) Rhesus macaques. The systemic behavioral experiments were performed with seven aged (18–30 years) Rhesus macaques (2 male, 5 female). Subjects were individually or pair-housed with 12-hour light cycles in humidity and temperature-controlled environments. The immunoelectron microscopy experiments were performed with four adult Rhesus macaques (10–22 y.o., female). All procedures were conducted in accordance with NIH guidelines and approved by the Yale University IACUC.

METHOD DETAILS

Immunoelectron Microscopy

Tissue Preparation: Four adult Rhesus macaques (10–22 y.o., female) were anesthetized with sodium pentobarbital (100 mg/kg, i.v.), and perfused transcardially with oxygenated artificial cerebrospinal fluid, followed by 4% paraformaldehyde, 0.05% glutaraldehyde, and 0.18% picric acid in 0.1 M phosphate buffer (Campbell et al.). Brain tissue was blocked coronally and vibrosliced at 60–70 μm in PB, cryoprotected in sucrose, immersed in liquid nitrogen, and stored at −80°C. Sections from dlPFC (Walker's area 46) were then processed for M1R and KCNQ with peroxidase or silver-enhanced 1.4nm gold for single immunocytochemistry. Non-specific reactivity was suppressed with 10% non-immune goat serum (NGS), and 5% IgG-free bovine serum albumin

(BSA) in 50mM Tris-buffered saline (TBS). Normal sera and BSA were purchased from Jackson Immunoresearch (West Grove, PA, United States of America). All chemicals and supplies for electron microscopy were purchased from Sigma Aldrich (St. Louis, MO, United States of America) and Electron Microscopy Sciences (Hatfield, PA, United States of America), respectively. All immunoprocedures as well as processing for electron microscopy have been described previously (Paspalas et al, 2013, Jin et al 2017).

Peroxidase/Gold Single Immunocytochemisry: For immunoperoxidase labeling, sections were incubated for 72 h at 4˚C with the M1 receptor antibody or KCNQ5 antibody in TBS with 1% NGS, and transferred for 2 h at room temperature to species-specific biotinylated $F(ab')_2$ fragments in TBS, and finally to avidin-biotinylated peroxidase (1:200 in TBS; Vector Laboratories, Burlingame, CA, United States of America) for 2 h at room temperature. Peroxidase activity was visualized in 0.025% diaminobenzidine (DAB) in TB with the addition of 0.005% hydrogen peroxide for 8–12 min. The omission of the primary antibody or substitution with non-immune serum abolished all reactivity.

For immunogold labeling, KCNQ2, KCNQ3 and KCNQ5 antibodies were diluted in TBS with 2% NGS (N-TBS), and applied for 36 h at 4°C. Sections were washed in N-TBS supplemented with 0.07% Tween 20 and 0.1% BSA-c gold-buffer, and incubated for 2 h at RT with species-specific Fab' conjugated to 1.4 nm gold cluster (1:200; Nanoprobes). Following fixation in buffered glutaraldehyde in PB, gold was enhanced under a mercury-vapor safelight for 8–10 min on ice with a silver autometallographic developer (HQ Silver; Nanoprobes, Yaphank, NY, United States of America). The peroxidase and gold immunoprocedures have been described in detail previously (Jin et al., 2017; Paspalas et al., 2018; Paspalas et al., 2013).

Electron Microscopy: All sections were processed as previously described (Paspalas and Goldman-Rakic, 2005; Paspalas et al 2013; Jin et al. 2017). Briefly, blocks containing dlPFC layer III were sampled for re-sectioning and analysis. The specimens were cut into 50nm sections using an ultramicrotome (Leica, Norcross, GA, United States of America) and analyzed under a JEM1010 (Jeol, Tokyo, Japan) transmission electron microscope at 80 kV. Several plastic blocks of each brain were examined using the 4^{th} to 20^{th} surface most sections of each block (i.e., 200–1000 nm), avoiding penetration artifacts. Structures were digitally captured at x25,000-x100,000 magnification with a Bioscan camera (Gatan, Pleasanton, CA, United States of America) and individual panels were adjusted for brightness and contrast using Adobe Photoshop and Illustrator CC.2017.01 image editing software (Adobe Systems Inc., San Jose, CA, United States of America). Approximately, 600 micrographs of selected areas of neuropil with immunopositive profiles were used for analysis. For profile identification, we adopted the criteria summarized by Peters (Peters et al., 1991).

Electrophysiology and Iontophoresis

Oculomotor delayed response (ODR) task: Rhesus macaques were trained to perform an ODR task, a test of visuospatial working memory. The task requires the subject to make a memory guided saccade to a remembered visuospatial location for a juice reward. The task is illustrated in Fig.1A. A central light is illuminated on an LED display monitor, serving as a fixation target. To initiate a trial the subject maintains fixation at the central spot for 0.5s (fixation period). Following this fixation, a cue is illuminated for 0.5s (cue period) at 1 of 8 peripheral targets located at an eccentricity of 13° with respect to the fixation spot. After the cue is extinguished, a 2.5s delay period follows (delay period). The subject is required to maintain fixation on the central spot throughout both the cue presentation and the delay period. At the end of the delay period the fixation spot is extinguished, instructing the animal to make a memory-guided saccade to the remembered location. A trial was considered successful if the animal made a saccade to the area within 2° around the previously cued location within 0.5s after the offset of the fixation spot. If completed successfully the animal was rewarded with juice immediately after the successful response. The inter-trial interval was 3s. The animal's eye position was monitored with ISCAN Eye Movement Monitoring System, and the ODR task was generated by PictoBox System (developed by Dr. Daeyeol Lee and colleagues, Yale University).

Recording Site: Animals underwent a magnetic resonance imaging (MRI) brain scan to obtain the exact anatomical coordinates of the desired recording site over the caudal principal sulcus of cortical area 46 shown in Fig.1C. These coordinates were then used to guide placement of the chronic recording chambers and electrophysiological recordings.

Recording and Iontophoresis: Electrodes for dual recording and iontophoresis were constructed with a 20μm-pitch carbon fiber inserted into the central barrel of a 7-barrel nonfilamented capillary glass (Friedrich and Dimmock). The assembly was pulled using a custom electrode puller (PMP-107, Microdata Instrument Inc.) and the tip was beveled to reach impedances of 0.3–1.0 MΩ with tip sizes of 30–40μm. The outer 6 barrels of the electrode were then filled with up to 3 different drug solutions (2 consecutive barrels for each drug), which were pushed through the tip of the electrode using air. A Neurophore BH2 iontophoretic system (Medical Systems Corp.) was used to deliver the drugs. Drugs were ejected at currents that varied from 5nA – 60nA. Retaining currents of 5nA at the opposite polarity were used in a cycled manner (1s ON, 1s OFF) when not applying drugs. Drug ejection did not create noise in the recording, and there was no iontophoresis-related change in spike waveforms at any ejection current. The pharmacological agents used for iontophoresis can be found in the Key Resources Table. Each compound was dissolved at 0.01 M concentration in either sterile water or saline with pH 3–4.

The electrode was mounted on a MO-95 micromanipulator (Narishige, East Meadow, NY) in a 25-guage stainless steel guide tube. *Dura mater* was punctured using the guide tube to enable access of the electrode to cortex. Extra-cellular voltage was amplified using an AC/DC differential preamplifier (Model 3000, A-M SYSTEMS) and band-pass filtered (180Hz-6Hz, 20dB gain, 4-pole Butterworth; Kron-Hite, Avon, MA). Signals were digitized (15kHz; micro 1401, Cambridge Electronics Design, Cambridge, UK) and acquired using the Spike2 software (CED, Cambridge, UK). Neuronal activity was analyzed using waveform sorting by a template-matching algorithm. Post-stimulus time histograms (PSTHs) and rasters were constructed online to determine the relationship of unit activity to the task. Unit activity was measured in spikes per second. If the rasters showed that a neuron displayed task-related activity, recording continued and pharmacological testing was performed.

Neuronal activities were first collected from the cell under a control condition in which at least eight trials at each of eight cue locations were obtained. A typical Delay cell is shown in Figure 1D. Upon establishing the stability of the cells' activity, this control condition was followed by iontophoretic application of drug(s). Dose-dependent effects of the drug were tested in two or more consecutive conditions, followed by a Recovery condition or a Reversal condition. Drugs were continuously applied at a relevant current throughout a given condition. Each condition had ~8 (6–12) trials at each location to allow for statistical analyses of drug effects.

Behavioral Testing—The effects of systemically administered VU0453595 were assessed in aged (18–30 years) Rhesus macaques (2 male, 5 female). This positive allosteric modulator (PAM) for M1 was developed and purchased directly from the Conn group at Vanderbilt University (Nashville, TN) (Ghoshal et al., 2016). Monkeys were trained on a

manual, multiple delay spatial working memory task in a Wisconsin General Testing Apparatus. The experimenter placed a food reward in 1 of 2 wells while the animal watched. Both wells were then covered with identical cardboard plaques and an opaque screen was lowered for a variable delay period. The screen was raised at the end of the delay and the animal had to point to the correct well to receive the food reward. Reward was quasi-randomly distributed between the left and right wells, and a daily test session had 30 trials. Five different delay lengths (designated A, B, C, D, and E delays) were quasi-randomly distributed during a single test session across the 30 trials. The delay length was adjusted for each animal so they had a stable baseline performance of 60–80% correct, varying from 1–12 seconds (where delay length A = 0 sec delay, B = 1*delay, C = 2* delay, etc). Animals testing above 80% correct over multiple days at 12 seconds were returned to a 1 second delay with a higher number of choice wells (beginning with 2 wells). An animal received drug treatments if it had a baseline performance for 2 consecutive testing sessions. The aged animals used had no significant working memory impairments compared to the younger adult animals, though the aged monkeys had spent many more years performing this task, which is an important confound.

Monkeys received VU0453595 (0.0001–10.0μg/kg) 60 minutes before testing administered via intramuscular injection. Drug was dissolved in a vehicle solution of 10% TWEEN in sterile water. Monkeys were tested by experimenters blind to drug versus vehicle conditions, with washout periods of at least 10 days between drug treatments.

QUANTIFICATION AND STATISTICAL ANALYSIS

Electrophysiology Data Analyses—Each trial in the ODR task was divided into four epochs – initial Fixation, Cue, Delay and Response (Saccade). The initial Fixation epoch lasted for 0.5 sec. The Cue epoch lasted for 0.5 sec and corresponds to the stimulus presentation phase of the task. The Delay lasted for 2.5 sec and reflects the mnemonic component of the task. The Response phase started immediately after the Delay epoch and lasted ~1.5 sec. Data analysis was performed in MATLAB, SPSS and GraphPad Prism 7.01. This study focused on Delay cells that represent working memory. Many Delay cells fire during the cue and/or response epochs as well as the delay epoch; given their variable responses to the cue and response epochs, data analyses focused on the delay epoch. Unpaired t-test with Welch's correction and one-way ANOVA were employed to assess the effects of drug application on task-related activity or each single Delay cell Two-tailed paired t-test t or repeated measures one-way ANOVA with Turkey's multiple comparisons or repeated measures two-way ANOVA with Sidak's multiple comparisons were employed to assess the effects of drug application on task-related activity for the population analysis. In the interest of brevity, figures often show the neurons' preferred direction in comparison to just one non-preferred direction, the "anti-preferred" direction directly opposed to the neurons' preferred direction. For Delay cells, the spatial tuning was assessed by comparing firing levels for the neuron's preferred direction vs. its non-preferred directions. Quantification of spatial tuning was performed by calculating a measure of d' using the formula:

$$d' = (mean_{pref} - mean_{nonpref})/\sqrt{(sd^2_{pref} + sd^2_{nonpref})/2}$$

Behavioral Analysis—Data were analyzed using SPSS Statistics v26 (IBM). Drug effects were tested with 1-way ANOVA-R with paired comparisons, and 2-tailed paired-samples t-test. $P < 0.05$ was predetermined as the threshold for statistical significance.

DATA AND CODE AVAILABILITY—The datasets supporting the current study are available from the corresponding author on request.

Supplementary Material

Refer to Web version on PubMed Central for supplementary material.

Acknowledgements

We thank Dr. Jeffery Conn for providing the novel M1R positive allosteric modulator VU0453595 used for systemic behavioral testing. We also thank L Ciavarella, S Johnson, T Sadlon, M Wilson and M Horn for their invaluable technical support. This work was supported by National Institutes of Health R01 MH093354 to M.W., Brain & Behavior Research Foundation Young Investigator to Y.Y., and 1RL1AA017536 within U54RR024350 to A.A.

REFERENCES

Arnsten AFT, Jin LE, Gamo NJ, Ramos B, Paspalas CD, Morozov YM, Kata A, Bamford NS, Yeckel MF, Kaczmarek LK, El-Hassar L (2019) Role of KNQ potassium channels in stress-induced deficit of working memory. Neurobiol of Stress 11, 100187.

Arnsten AF, and Wang M (2016). Targeting Prefrontal Cortical Systems for Drug Development: Potential Therapies for Cognitive Disorders. Annu Rev Pharmacol Toxicol 56, 339–360. [PubMed: 26738476]

Barch DM, and Smith E (2008). The cognitive neuroscience of working memory: relevance to CNTRICS and schizophrenia. Biol Psychiatry 64, 11–17. [PubMed: 18400207]

Bartus RT, and Dean RL (1988). Tetrahydroaminoacridine, 3,4 diaminopyridine and physostigmine: direct comparison of effects on memory in aged primates. Neurobiol Aging 9, 351–356. [PubMed: 3185853]

Bartus RT, Dean RL 3rd, Beer B, and Lippa AS (1982). The cholinergic hypothesis of geriatric memory dysfunction. Science 217, 408–414. [PubMed: 7046051]

Berry AS, Demeter E, Sabhapathy S, English BA, Blakely RD, Sarter M, and Lustig C (2014). Disposed to distraction: genetic variation in the cholinergic system influences distractibility but not time-on-task effects. J Cogn Neurosci 26, 1981–1991. [PubMed: 24666128]

Birnbaum SG, Yuan PX, Wang M, Vijayraghavan S, Bloom AK, Davis DJ, Gobeske KT, Sweatt JD, Manji HK, and Arnsten AF (2004). Protein kinase C overactivity impairs prefrontal cortical regulation of working memory. Science 306, 882–884. [PubMed: 15514161]

Borsotto M, Cavarec L, Bouillot M, Romey G, Macciardi F, Delaye A, Nasroune M, Bastucci M, Sambucy JL, Luan JJ, et al. (2007). PP2A-Bgamma subunit and KCNQ2 K+ channels in bipolar disorder. Pharmacogenomics J 7, 123–132. [PubMed: 16733521]

Bowen DM, Smith CB, White P, and Davison AN (1976). Neurotransmitter-related enzymes and indices of hypoxia in senile dementia and other abiotrophies. Brain 99, 459–496. [PubMed: 11871]

Brown DA (2008). Kv7 (KCNQ) potassium channels that are mutated in human diseases. J Physiol 586, 1781–1783. [PubMed: 18381340]

Bussiere T, Giannakopoulos P, Bouras C, Perl DP, Morrison JH, and Hof PR (2003a). Progressive degeneration of nonphosphorylated neurofilament protein-enriched pyramidal neurons predicts

cognitive impairment in Alzheimer's disease: stereologic analysis of prefrontal cortex area 9. J Comp Neurol 463, 281–302. [PubMed: 12820162]

Bussiere T, Gold G, Kovari E, Giannakopoulos P, Bouras C, Perl DP, Morrison JH, and Hof PR (2003b). Stereologic analysis of neurofibrillary tangle formation in prefrontal cortex area 9 in aging and Alzheimer's disease. Neuroscience 117, 577–592. [PubMed: 12617964]

Campbell C, Grapov D, Fiehn O, Chandler CJ, Burnett DJ, Souza EC, Casazza GA, Gustafson MB, Keim NL, Newman JW, et al. (2014). Improved metabolic health alters host metabolism in parallel with changes in systemic xeno-metabolites of gut origin. PLoS One 9, e84260.

Cannon TD, Glahn DC, Kim J, Van Erp TG, Karlsgodt K, Cohen MS, Nuechterlein KH, Bava S, and Shirinyan D (2005). Dorsolateral prefrontal cortex activity during maintenance and manipulation of information in working memory in patients with schizophrenia. Arch Gen Psychiatry 62, 1071–1080. [PubMed: 16203952]

Clark S, Antell A, and Kaufman K (2015). New antiepileptic medication linked to blue discoloration of the skin and eyes. Ther Adv Drug Saf 6, 15–19. [PubMed: 25642319]

Condy C, Wattiez N, Rivaud-Pechoux S, Tremblay L, and Gaymard B (2007). Antisaccade deficit after inactivation of the principal sulcus in monkeys. Cereb Cortex 17, 221–229. [PubMed: 16481562]

Croxson PL, Kyriazis DA, and Baxter MG (2011). Cholinergic modulation of a specific memory function of prefrontal cortex. Nat Neurosci 14, 1510–1512. [PubMed: 22057191]

Dean B, McLeod M, Keriakous D, McKenzie J, and Scarr E (2002). Decreased muscarinic1 receptors in the dorsolateral prefrontal cortex of subjects with schizophrenia. Mol Psychiatry 7, 1083–1091. [PubMed: 12476323]

Delmas P, and Brown DA (2005). Pathways modulating neural KCNQ/M (Kv7) potassium channels. Nat Rev Neurosci 6, 850–862. [PubMed: 16261179]

Dhande OS, Bhatt S, Anishchenko A, Elstrott J, Iwasato T, Swindell EC, Xu HP, Jamrich M, Itohara S, Feller MB, and Crair MC (2012). Role of adenylate cyclase 1 in retinofugal map development. J Comp Neurol 520, 1562–1583. [PubMed: 22102330]

Disney AA, Aoki C, and Hawken MJ (2007). Gain modulation by nicotine in macaque v1. Neuron 56, 701–713. [PubMed: 18031686]

Dumitriu D, Hao J, Hara Y, Kaufmann J, Janssen WG, Lou W, Rapp PR, and Morrison JH (2010). Selective changes in thin spine density and morphology in monkey prefrontal cortex correlate with aging-related cognitive impairment. J Neurosci 30, 7507–7515. [PubMed: 20519525]

Elston GN, Benavides-Piccione R, Elston A, Zietsch B, Defelipe J, Manger P, Casagrande V, and Kaas JH (2006). Specializations of the granular prefrontal cortex of primates: implications for cognitive processing. Anat Rec A Discov Mol Cell Evol Biol 288, 2635.

Everling S, and DeSouza JF (2005). Rule-dependent activity for prosaccades and antisaccades in the primate prefrontal cortex. J Cogn Neurosci 17, 1483–1496. [PubMed: 16197701]

Freedman R, Olincy A, Buchanan RW, Harris JG, Gold JM, Johnson L, Allensworth D, Guzman-Bonilla A, Clement B, Ball MP, et al. (2008). Initial phase 2 trial of a nicotinic agonist in schizophrenia. Am J Psychiatry 165, 1040–1047. [PubMed: 18381905]

Funahashi S, Bruce CJ, and Goldman-Rakic PS (1989). Mnemonic coding of visual space in the monkey's dorsolateral prefrontal cortex. J Neurophysiol 61, 331–349. [PubMed: 2918358]

Galimberti D, and Scarpini E (2016). Old and new acetylcholinesterase inhibitors for Alzheimer's disease. Expert Opin Investig Drugs 25, 1181–1187.

Geula C, and Mesulam MM (1989). Cortical cholinergic fibers in aging and Alzheimer's disease: a morphometric study. Neuroscience 33, 469–481. [PubMed: 2636703]

Gibson GE, and Peterson C (1981). Aging decreases oxidative metabolism and the release and synthesis of acetylcholine. J Neurochem 37, 978–984. [PubMed: 7320734]

Gibson GE, Peterson C, and Jenden DJ (1981). Brain acetylcholine synthesis declines with senescence. Science 213, 674–676. [PubMed: 7256270]

Goldman-Rakic PS (1995). Cellular basis of working memory. Neuron 14, 477–485. [PubMed: 7695894]

Goldman PS, Rosvold HE, Vest B, and Galkin TW (1971). Analysis of the delayed-alternation deficit produced by dorsolateral prefrontal lesions in the rhesus monkey. J Comp Physiol Psychol 77, 212–220. [PubMed: 5000659]

Gonzalez-Burgos G, Barrionuevo G, and Lewis DA (2000). Horizontal synaptic connections in monkey prefrontal cortex: an in vitro electrophysiological study. Cereb Cortex 10, 82–92. [PubMed: 10639398]

Ghoshal A, Rook JM, Dickerson JW, Roop GN, Morrison RD, Jalan-Sakrikar N, Lamsal A, Noetzel MJ, Poslusney MS, Wood MR, et al. (2016). Potentiation of M1 muscarinic receptor reverses plasticity deficits and negative and cognitive symptoms in a schizophrenia mouse model. Neuropsychopharm 41, 598–610.

Green A, Ellis KA, Ellis J, Bartholomeusz CF, Ilic S, Croft RJ, Phan KL, and Nathan PJ (2005). Muscarinic and nicotinic receptor modulation of object and spatial n-back working memory in humans. Pharmacol Biochem Behav 81, 575–584. [PubMed: 15936063]

Gritton HJ, Howe WM, Mallory CS, Hetrick VL, Berke JD, and Sarter M (2016). Cortical cholinergic signaling controls the detection of cues. Proc Natl Acad Sci U S A 113, E1089–1097. [PubMed: 26787867]

Grothe M, Heinsen H, and Teipel S (2013). Longitudinal measures of cholinergic forebrain atrophy in the transition from healthy aging to Alzheimer's disease. Neurobiol Aging 34, 1210–1220. [PubMed: 23158764]

Grothe M, Heinsen H, and Teipel SJ (2012). Atrophy of the cholinergic Basal forebrain over the adult age range and in early stages of Alzheimer's disease. Biol Psychiatry 71, 805–813. [PubMed: 21816388]

Guan ZZ, Zhang X, Blennow K, and Nordberg A (1999). Decreased protein level of nicotinic receptor alpha7 subunit in the frontal cortex from schizophrenic brain. Neuroreport 10, 1779–1782. [PubMed: 10501574]

Gunthorpe MJ, Large CH, and Sankar R (2012). The mechanism of action of retigabine (ezogabine), a first-in-class K+ channel opener for the treatment of epilepsy. Epilepsia 53, 412–424. [PubMed: 22220513]

Hughes JR, Hatsukami DK, Mitchell JE, and Dahlgren LA (1986). Prevalence of smoking among psychiatric outpatients. Am J Psychiatry 143, 993–997. [PubMed: 3487983]

Iyengar R (1993). Molecular and functional diversity of mammalian Gs-stimulated adenylyl cyclases. FASEB J 7, 768–775. [PubMed: 8330684]

Jin LE, Wang M, Yang ST, Yang Y, Galvin VC, Lightbourne TC, Ottenheimer D, Zhong Q, Stein J, Raja A, et al. (2017). mGluR2/3 mechanisms in primate dorsolateral prefrontal cortex: evidence for both presynaptic and postsynaptic actions. Mol Psychiatry 22, 1615–1625. [PubMed: 27502475]

Jones BE (1993). The organization of central cholinergic systems and their functional importance in sleep-waking states. Prog Brain Res 98, 61–71. [PubMed: 8248538]

Kaminsky Z, Jones I, Verma R, Saleh L, Trivedi H, Guintivano J, Akman R, Zandi P, Lee RS, and Potash JB (2015). DNA methylation and expression of KCNQ3 in bipolar disorder. Bipolar Disord 17, 150–159. [PubMed: 25041603]

Keefe RS, Meltzer HA, Dgetluck N, Gawryl M, Koenig G, Moebius HJ, Lombardo I, and Hilt DC (2015). Randomized, Double-Blind, Placebo-Controlled Study of Encenicline, an alpha7 Nicotinic Acetylcholine Receptor Agonist, as a Treatment for Cognitive Impairment in Schizophrenia. Neuropsychopharmacology 40, 3053–3060. [PubMed: 26089183]

Kim EC, Patel J, Zhang J, Soh H, Rhodes JS, Tzingounis AV, and Chung HJ (2019). Heterozygous loss of epilepsy gene KCNQ2 alters social, repetitive and exploratory behaviors. Genes Brain Behav, e12599.

Lehman A, Thouta S, Mancini GMS, Naidu S, van Slegtenhorst M, McWalter K, Person R, Mwenifumbo J, Salvarinova R, Study C, et al. (2017). Loss-of-Function and Gain-of-Function Mutations in KCNQ5 Cause Intellectual Disability or Epileptic Encephalopathy. Am J Hum Genet 101, 65–74. [PubMed: 28669405]

Major AJ, Vijayraghavan S, and Everling S (2015). Muscarinic Attenuation of Mnemonic Rule Representation in Macaque Dorsolateral Prefrontal Cortex during a Pro- and Anti-Saccade Task. J Neurosci 35, 16064–16076. [PubMed: 26658860]

Major AJ, Vijayraghavan S, and Everling S (2018). Cholinergic Overstimulation Attenuates Rule Selectivity in Macaque Prefrontal Cortex. J Neurosci 38, 1137–1150. [PubMed: 29255006]

Mesulam MM, Mufson EJ, Levey AI, and Wainer BH (1983). Cholinergic innervation of cortex by the basal forebrain: cytochemistry and cortical connections of the septal area, diagonal band nuclei, nucleus basalis (substantia innominata), and hypothalamus in the rhesus monkey. J Comp Neurol 214, 170–197. [PubMed: 6841683]

Mesulam MM, Mufson EJ, and Rogers J (1987). Age-related shrinkage of cortically projecting cholinergic neurons: a selective effect. Ann Neurol 22, 31–36. [PubMed: 3307603]

Mesulam MM, Volicer L, Marquis JK, Mufson EJ, and Green RC (1986). Systematic regional differences in the cholinergic innervation of the primate cerebral cortex: distribution of enzyme activities and some behavioral implications. Ann Neurol 19, 144–151. [PubMed: 3963756]

Miceli F, Striano P, Soldovieri MV, Fontana A, Nardello R, Robbiano A, Bellini G, Elia M, Zara F, Taglialatela M, and Mangano S (2015). A novel KCNQ3 mutation in familial epilepsy with focal seizures and intellectual disability. Epilepsia 56, e15–20. [PubMed: 25524373]

Morrison JH, and Hof PR (2007). Life and death of neurons in the aging cerebral cortex. Int Rev Neurobiol 81, 41–57. [PubMed: 17433917]

Mrzljak L, Levey AI, and Goldman-Rakic PS (1993). Association of m1 and m2 muscarinic receptor proteins with asymmetric synapses in the primate cerebral cortex: morphological evidence for cholinergic modulation of excitatory neurotransmission. Proc Natl Acad Sci U S A 90, 5194–5198. [PubMed: 8389473]

Parikh V, Kozak R, Martinez V, and Sarter M (2007). Prefrontal acetylcholine release controls cue detection on multiple timescales. Neuron 56, 141–154. [PubMed: 17920021]

Paspalas CD, Carlyle BC, Leslie S, Preuss TM, Crimins JL, Huttner AJ, van Dyck CH, Rosene DL, Nairn AC, and Arnsten AFT (2018). The aged rhesus macaque manifests Braak stage III/IV Alzheimer's-like pathology. Alzheimers Dement 14, 680–691. [PubMed: 29241829]

Paspalas CD and Goldman-Rakic PS (2005). Presynaptic D1 dopamine receptors in primate prefrontal cortex: Target-specific expression in the glutamatergic synapse. J Neurosci 25, 1260–1267. [PubMed: 15689564]

Paspalas CD, Wang M, and Arnsten AF (2013). Constellation of HCN channels and cAMP regulating proteins in dendritic spines of the primate prefrontal cortex: potential substrate for working memory deficits in schizophrenia. Cereb Cortex 23, 1643–1654. [PubMed: 22693343]

Perry EK, Blessed G, Tomlinson BE, Perry RH, Crow TJ, Cross AJ, Dockray GJ, Dimaline R, and Arregui A (1981). Neurochemical activities in human temporal lobe related to aging and Alzheimer-type changes. Neurobiol Aging 2, 251–256. [PubMed: 6174877]

Peters A, Josephson K, and Vincent SL (1991). Effects of aging on the neuroglial cells and pericytes within area 17 of the rhesus monkey cerebral cortex. Anat Rec 229, 384–398. [PubMed: 2024779]

Rapp PR, and Amaral DG (1989). Evidence for task-dependent memory dysfunction in the aged monkey. J Neurosci 9, 3568–3576. [PubMed: 2795141]

Schroeder BC, Kubisch C, Stein V, and Jentsch TJ (1998). Moderate loss of function of cyclic-AMP-modulated KCNQ2/KCNQ3 K+ channels causes epilepsy. Nature 396, 687–690. [PubMed: 9872318]

Suh BC, and Hille B (2002). Recovery from muscarinic modulation of M current channels requires phosphatidylinositol 4,5-bisphosphate synthesis. Neuron 35, 507–520. [PubMed: 12165472]

Suh BC, Horowitz LF, Hirdes W, Mackie K, and Hille B (2004). Regulation of KCNQ2/KCNQ3 current by G protein cycling: the kinetics of receptor-mediated signaling by Gq. J Gen Physiol 123, 663–683. [PubMed: 15173220]

Thiele A (2013). Muscarinic signaling in the brain. Annu Rev Neurosci 36, 271–294. [PubMed: 23841840]

Tikhonova TB, Miyamae T, Gulchina Y, Lewis DA, and Gonzalez-Burgos G (2018). Cell Type- and Layer-Specific Muscarinic Potentiation of Excitatory Synaptic Drive onto Parvalbumin Neurons in Mouse Prefrontal Cortex. eNeuro 5.

Veselinovic T, Vernaleken I, Janouschek H, Kellermann T, Paulzen M, Cumming P, and Grunder G (2015). Effects of anticholinergic challenge on psychopathology and cognition in drug-free patients with schizophrenia and healthy volunteers. Psychopharmacology (Berl) 232, 1607–1617. [PubMed: 25373869]

Vijayraghavan S, Major AJ, and Everling S (2018). Muscarinic M1 Receptor Overstimulation Disrupts Working Memory Activity for Rules in Primate Prefrontal Cortex. Neuron 98, 1256–1268 e1254.

Vijayraghavan S, Wang M, Birnbaum SG, Williams GV, and Arnsten AF (2007). Inverted-U dopamine D1 receptor actions on prefrontal neurons engaged in working memory. Nat Neurosci 10, 376–384. [PubMed: 17277774]

Wallis JD, Anderson KC, and Miller EK (2001). Single neurons in prefrontal cortex encode abstract rules. Nature 411, 953–956. [PubMed: 11418860]

Wang M, Gamo NJ, Yang Y, Jin LE, Wang XJ, Laubach M, Mazer JA, Lee D, and Arnsten AF (2011). Neuronal basis of age-related working memory decline. Nature 476, 210–213. [PubMed: 21796118]

Wang M, Ramos BP, Paspalas CD, Shu Y, Simen A, Duque A, Vijayraghavan S, Brennan A, Dudley A, Nou E, et al. (2007). Alpha2A-adrenoceptors strengthen working memory networks by inhibiting cAMP-HCN channel signaling in prefrontal cortex. Cell 129, 397410.

Wang M, Yang Y, Wang CJ, Gamo NJ, Jin LE, Mazer JA, Morrison JH, Wang XJ, and Arnsten AF (2013). NMDA receptors subserve persistent neuronal firing during working memory in dorsolateral prefrontal cortex. Neuron 77, 736–749. [PubMed: 23439125]

Wenk GL, Pierce DJ, Struble RG, Price DL, and Cork LC (1989). Age-related changes in multiple neurotransmitter systems in the monkey brain. Neurobiol Aging 10, 11–19. [PubMed: 2569169]

Yang Y, Paspalas CD, Jin LE, Picciotto MR, Arnsten AF, and Wang M (2013). Nicotinic alpha7 receptors enhance NMDA cognitive circuits in dorsolateral prefrontal cortex. Proc Natl Acad Sci U S A 110, 12078–12083. [PubMed: 23818597]

Highlights:

- "Delay" neurons in dorsolateral prefrontal cortex (dlPFC) subserve working memory
- Low dose muscarinic M1R stimulation enhances Delay firing in aged primate dlPFC
- This involves M1R closing KCNQ "m" channels, which localize on dendrites and spines
- Systemic administration of low doses of an M1R PAM also improved working memory

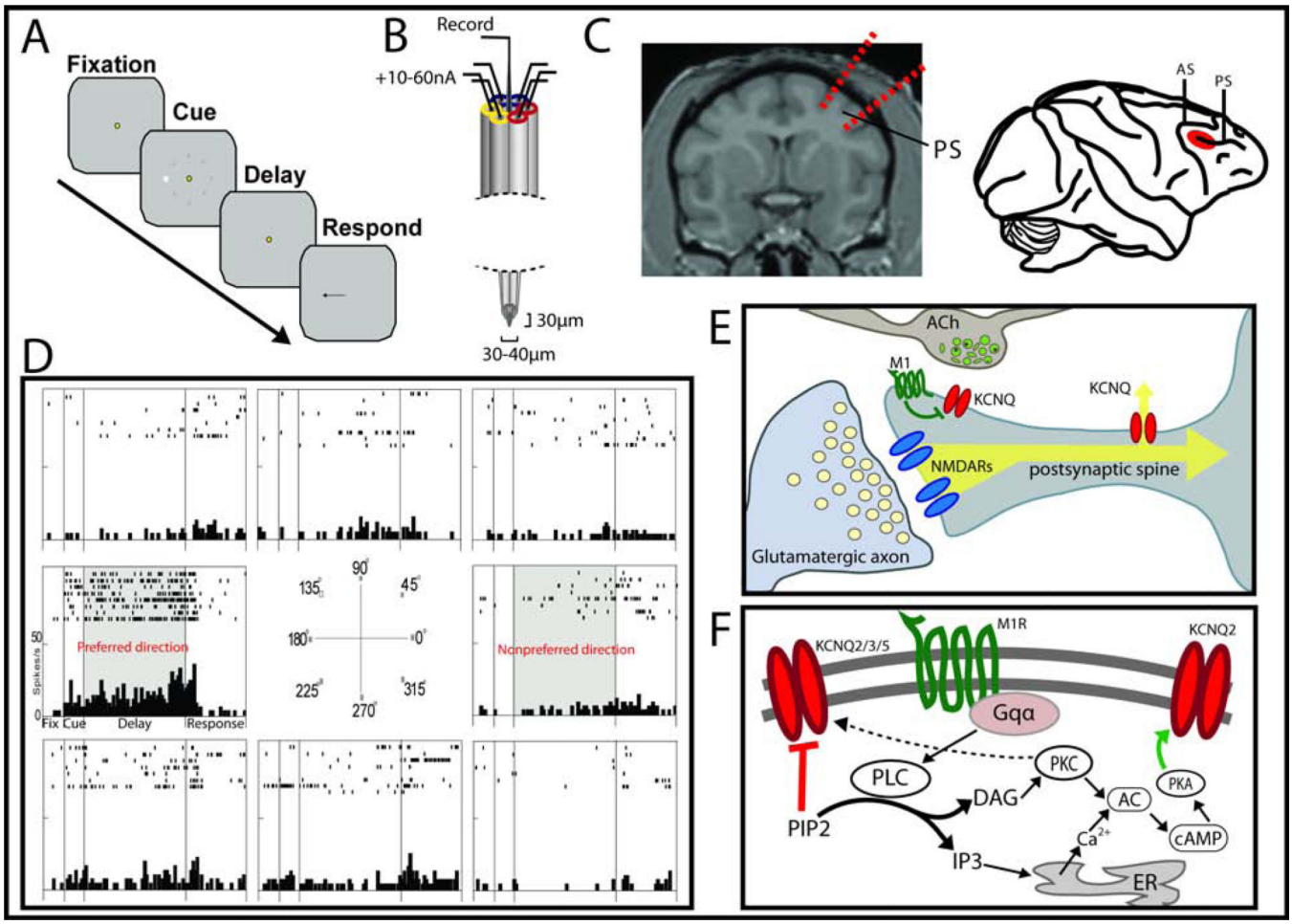

Figure 1: Electrophysiological recordings of Delay cells to probe M1R mechanisms.

A. The oculomotor delayed response (ODR) task. **B.** Cartoon of the seven barrel glass electrodes used for combined electrophysiology and iontophoresis *in vivo*. **C.** (Left) an MRI image indicating the site of chamber placement and recording. (Right) the location for recordings at the posterior end of the principle sulcus in the dlPFC (red oval). **D.** Example Delay cell showing elevated persistent activity selectively for the 180° location and not for the other randomly presented target locations. **E,F.** The working model of cholinergic activation of M1Rs postsynaptically on spines influencing neural membranes via two pathways.

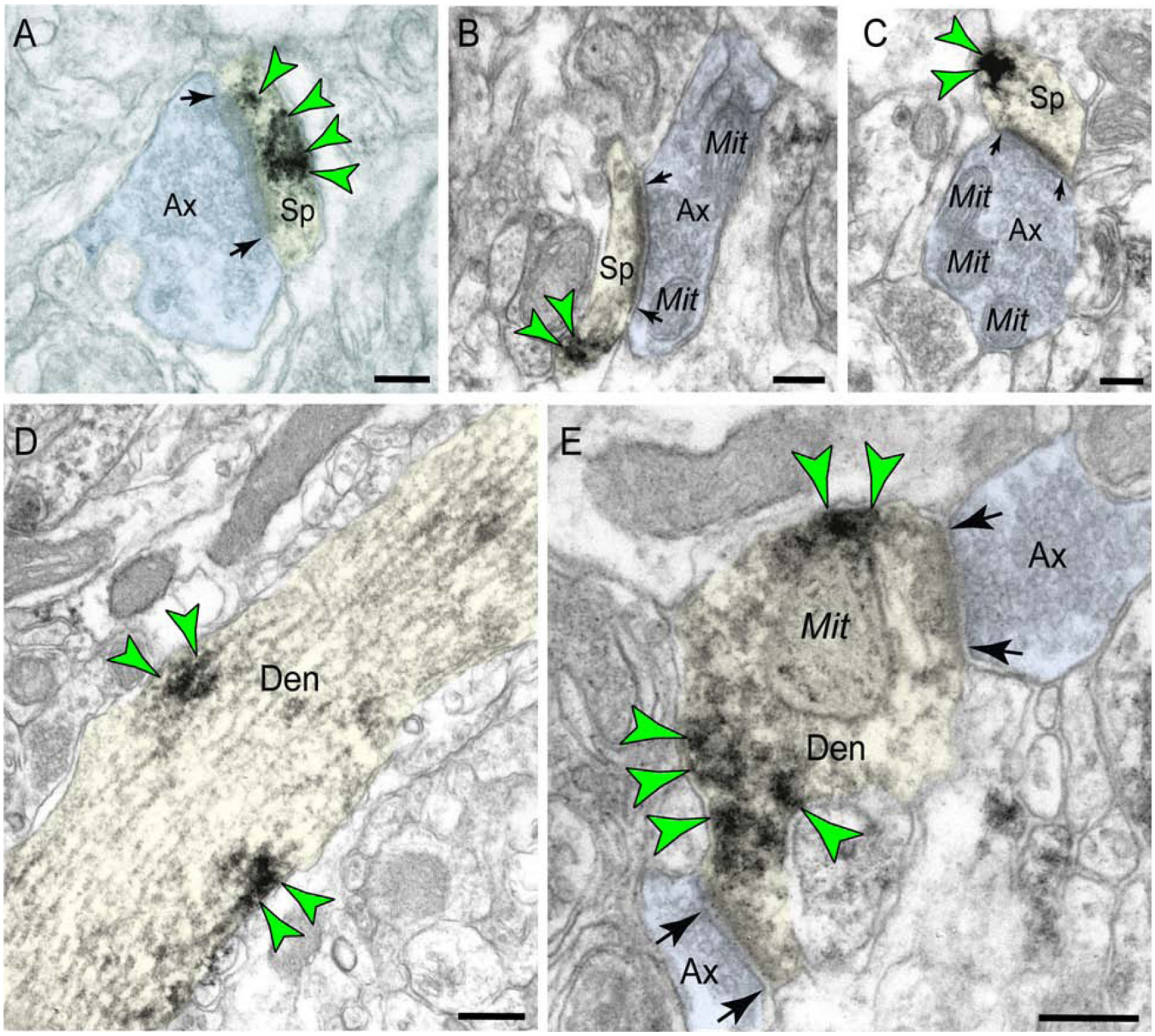

Figure 2: M1R localization in macaque dlPFC layer III.

(A-C) Postsynaptic M1R in dendritic spines in macaque dlPFC layer III is predominantly associated with the postsynaptic density (PSD) and observed in perisynaptic and extrasynaptic locations near the axospinous glutamatergic-like synapse. **(D)** M1R are often captured at the plasma membrane of pyramidal neuron dendritic shafts. **(E)** Postsynaptic M1R are also observed in putative GABAergic interneuron dendrites in association with the plasma membrane. Synapses are between arrows. Color-coded arrowheads (green) point to M1R immunoreactivity. Profiles are pseudocolored for clarity. Ax, axon; Sp, spine; Den, dendrite; Mit, mitochondria. Scale bars, 200 nm.

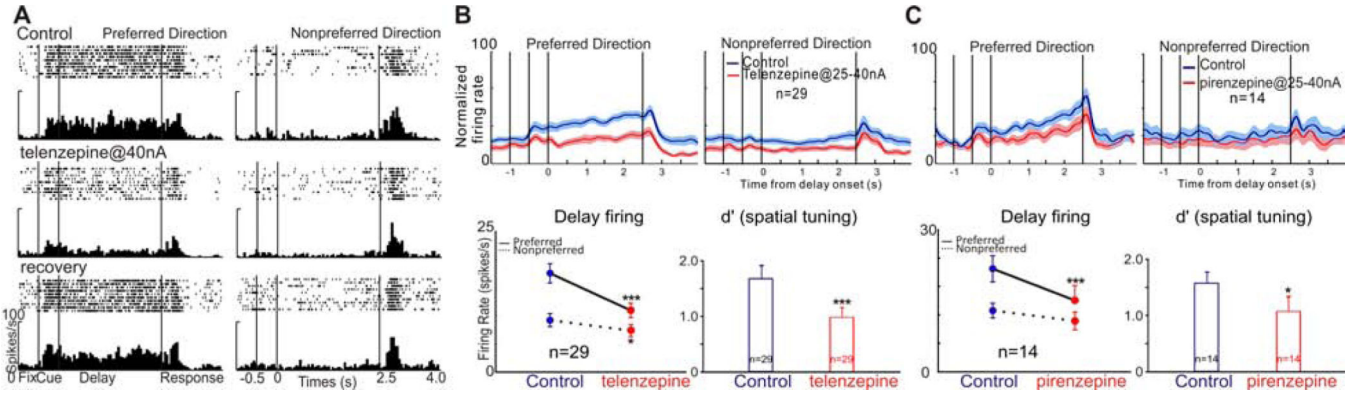

Figure 3: M1R blockade reduces delay-related firing and spatial tuning of dlPFC Delay cells.

A. Iontophoresis of the M1R antagonist, telen, markedly reduced delay firing, and firing was partially restored when telen application was terminated (recovery). **B**. Telen reduces delay-related firing and spatial tuning at the population level. Upper panel shows normalized average firing rates for 29 Delay cells. Bottom left shows the mean±SEM firing rate of 29 Delay cells during the Delay period of the task. Bottom right shows iontophoresis of telen significantly decreased the spatial tuning of Delay cells by decreasing d'. **C**. Piren reduces delay firing and spatial tuning at the population level. (*p<0.05; **p<0.01, ***p<0.001).

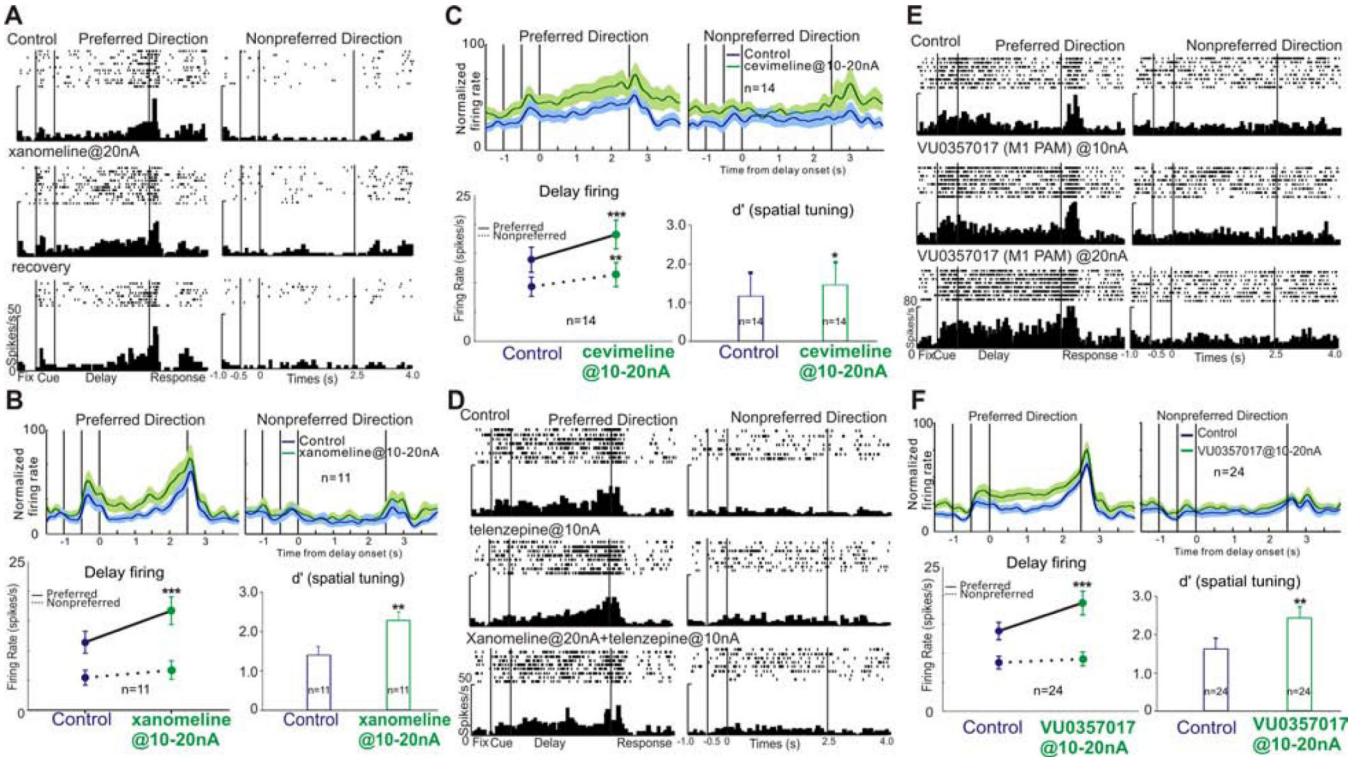

Figure 4. M1R stimulation enhances delay-related firing and spatial tuning of dlPFC Delay cells.

A. Iontophoresis of the M1R agonist, xano, significantly enhanced delay firing. Firing was reduced to control level after xano application was terminated. **B**. Xano enhances delay firing and spatial tuning at the population level. Upper panel shows normalized average firing rates for 11 Delay cells. Bottom left shows the mean±SEM firing rate of 11 Delay cells during the Delay period. Bottom right shows xano significantly increased the spatial tuning. **C**. Cevi enhances delay firing and spatial tuning at the population level. **D.** The M1R antagonist telen blocks the enhancement in delay firing with xano, supporting specificity of these effects from actions at M1Rs. **E**. The M1R PAM, VU0357017, significantly enhanced delay firing in a dose-dependent manner. **F**. The enhancing effects of VU0357017 on delay-related firing and spatial tuning at the population level (n=24). (*p<0.05; **p<0.01, ***p<0.001).

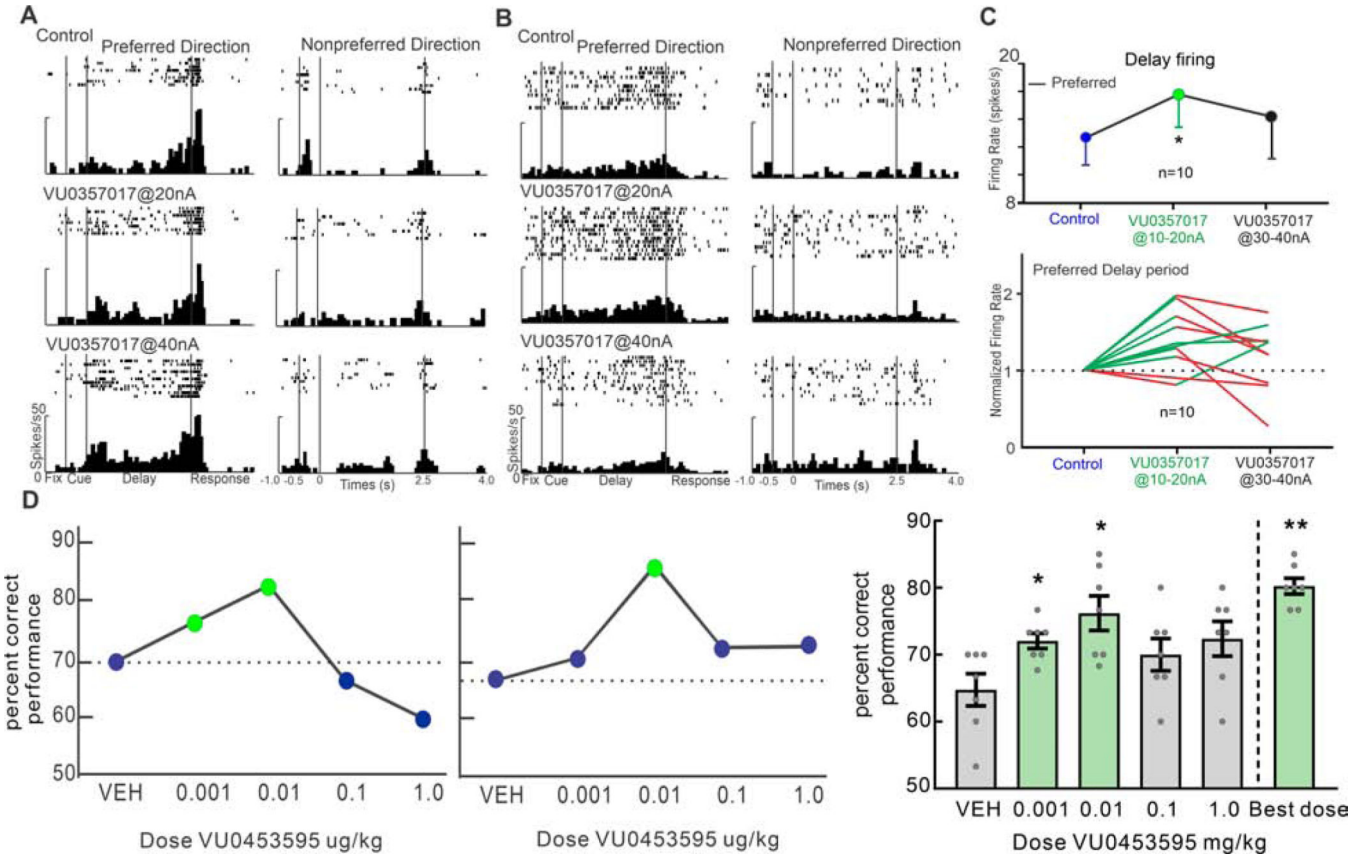

Figure 5. The mixed effects of higher M1R stimulation on delay-related firing of dlPFC Delay cells.

A. A single neuron example of an increase in delay firing at both low (20nA) and higher (40nA) doses of VU035. **B.** An example of an individual neuron with an inverted U dose response. VU035 at 20nA significantly increased delay firing, but subsequent application at 40nA decreased delay firing. **C.** M1R stimulation produces an inverted-U dose response in dlPFC Delay cells, where low doses enhance firing rates and higher doses decrease firing rates overall. **D.** Systemic application of VU0453595 improve primates working memory performance. Left and Middle: single dose-response curves from two individual macaque monkeys aged 23 (female, left) and aged 25 (male, middle). Right: mean±SEM of the behavioral response of 7 aged monkeys (age 19–31 years) across the dose range of VU0453595 tested (*p<0.05; **p<0.01).

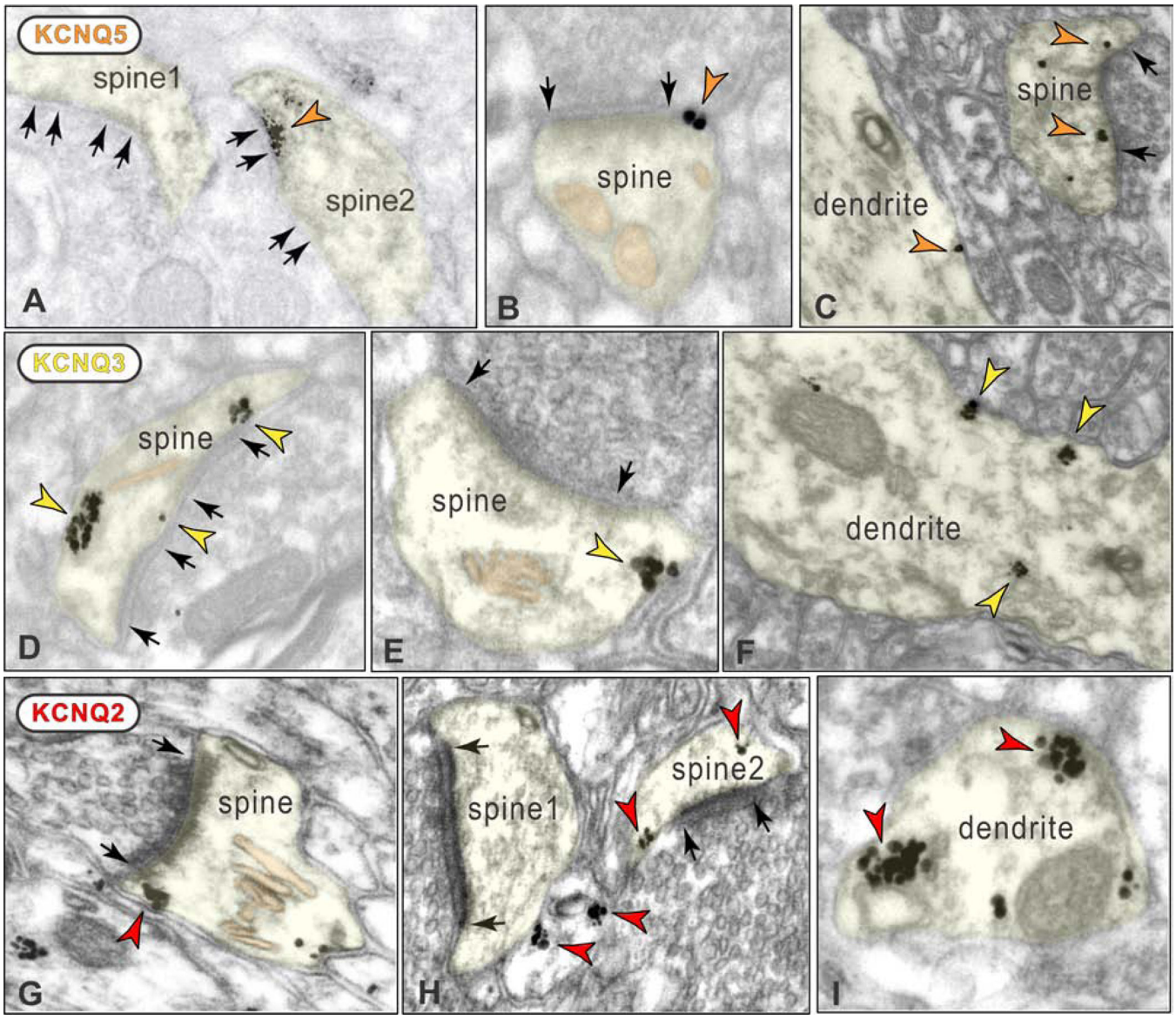

Figure 6. ImmunoEM localization of KCNQ isoforms on spines and dendrites in layer III dlPFC.

A-C. KCNQ5 localization on spines and dendrites. Panel A shows DAB KCNQ5 immunolabeling within the PSD in a perforated, asymmetric (glutamate-like) synapse (spine2); unlabeled synapses in spine1 and spine2 are indicated for comparison. Panel B shows immunogold KCNQ5 labeling immediately next to the PSD (peri-synaptic) in a spine. Panel C shows KCNQ5 immunogold peri-synaptic in a spine, and on the plasma membrane of a dendrite. **D-F.** KCNQ3 localization on spines and dendrites. Panel D shows KCNQ3 immunogold labeling in a spine with a perforated, asymmetric synapse. Panel E shows extrasynaptic KCNQ3 immunogold labeling in a spine receiving a glutamate-like asymmetric synapse. Panel F shows KCNQ3 immunogold labeling on the plasma membrane and within a dendrite. **G-I.** KCNQ2 localization on spines and dendrites. Panels G and H show KCNQ2 immunogold labeling in spines near synapses and at extrasynaptic locations. Panel H also shows label in an unidentified, likely glial profile. Panel I shows KCNQ2

immunogold labeling on the plasma membrane of a dendrite. Black arrows delineate synapses. The calcium-storing spine apparatus is pseudo-colored pink in panels B, D-E and G.

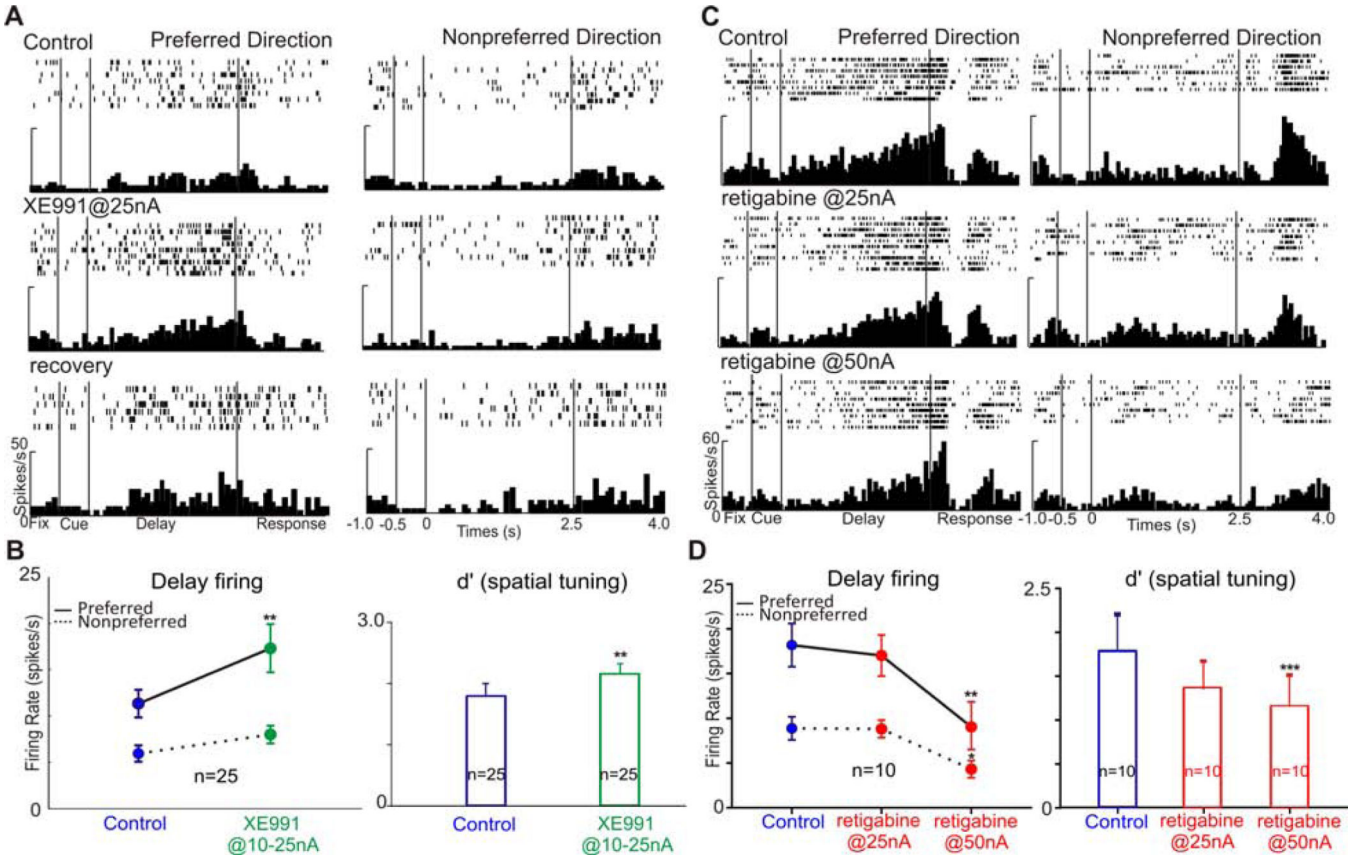

Figure 7. Blocking/opening KCNQ channels strengthens/reduces delay-related firing.

A. Iontophoresis of the KCNQ blocker, XE991, significantly enhanced delay-related firing. Firing was reduced to control level after XE991 was terminated. **B**. The enhancing effects of XE991 on delay firing and spatial tuning at the population level. The left shows XE991 significantly enhanced the delay firing. The right shows XE991 significantly increased the spatial tuning. **C**. Iontophoresis of the KCNQ activator, retigabine, reduced delay firing in a dose-dependent manner. **D**. The reducing effects of retigabine on delay firing and spatial tuning at the population level. The left shows retigabine significantly reduced the delay firing. The right shows retigabine significantly decreased the spatial tuning. (*p<0.05; **p<0.01, ***p<0.001; Data are represented as mean±SEM).

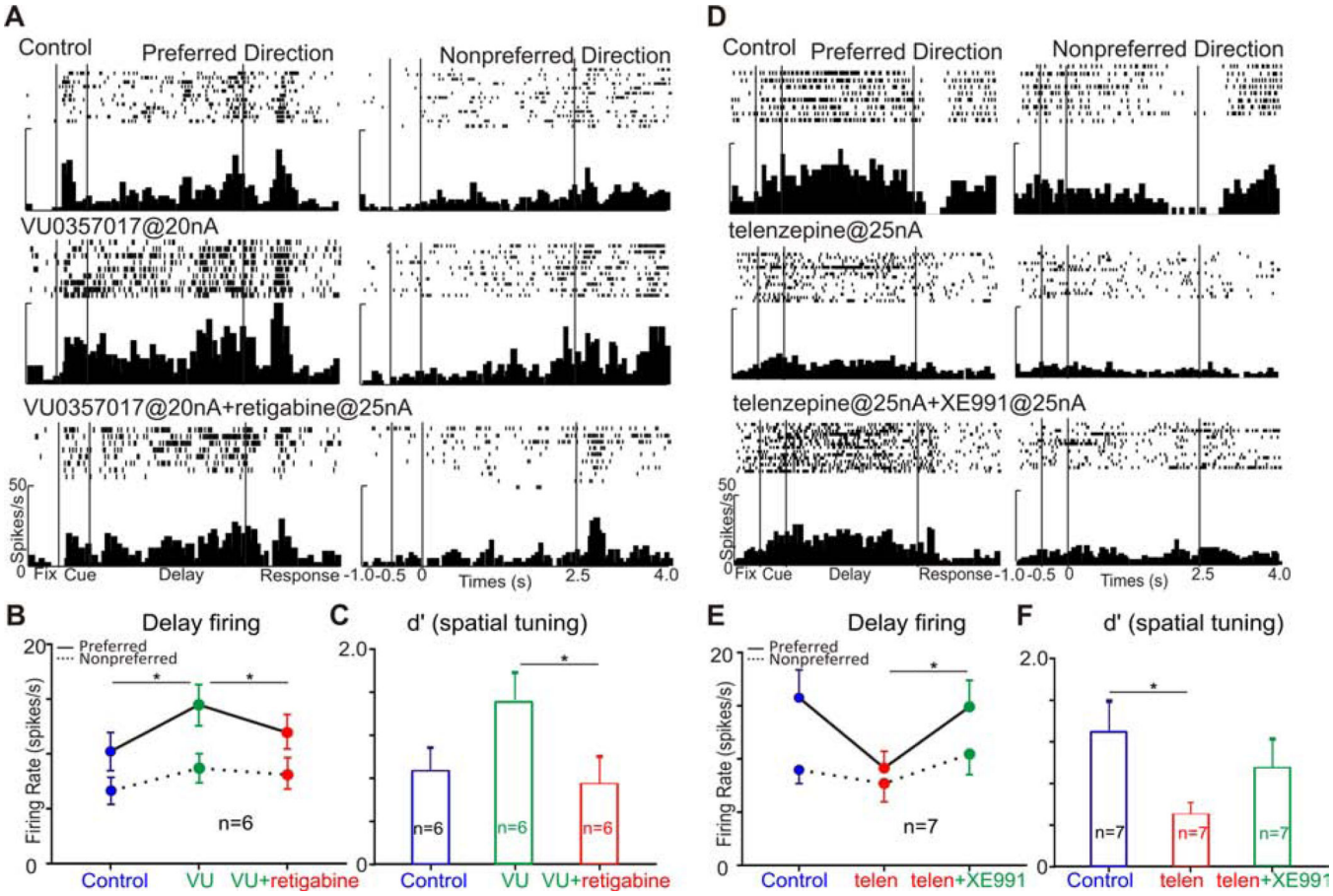

Figure 8. Opening KCNQ channels blocks the enhancement from M1R stimulation and closing KCNQ channels rescues the reduction from M1R blockade.

A. VU035 significantly enhanced delay firing, and retigabine blocked this enhancement when these two agents were co-applied. **B**. Retigabine significantly blocked the enhancement of VU035 at the population level. **C.** Retigabine blocked the enhancement of VU035 on spatial tuning. **D.** Telen dramatically reduced delay-related firing, and XE991 rescued the reduction of telen when these two agents were co-applied. **E.** XE991 significantly rescued the reduction of telen at the population level. **F.** XE991 rescued the reduction of telen on spatial tuning. (*p<0.05; **p<0.01, ***p<0.001; Data are represented as mean±SEM).

KEY RESOURCES TABLE

Chemicals and antibodies

REAGENT or RESOURCE	SOURCE	IDENTIFIER
M1 receptor antibody	Sigma Aldrich	Cat # M9808; RRID:AB_260731
KCNQ2 antibody N26A/23	Abcam	Cat # ab84812; RRID:AB_1859997
KCNQ2 antibody	Abcam	Cat # ab22897; RRID:AB_775890
KCNQ3 antibody	Abcam	Cat # ab66640; RRID:AB_2131709
KCNQ3 antibody	Abcam	Cat # ab16228; RRID:AB_302332
KCNQ5 antibody	Abcam	Cat # ab66740; RRID:AB_1139413
KCNQ5 antibody	Abcam	Cat# ab57634; RRID:AB_944919
Scopolamine	Tocris Bioscience	Cat # 1414; CAS # 114–49-8; PubChem CID # 45073445
Telenzepine	Tocris Bioscience	Cat # 1122; CAS # 147416–96-4; PubChem CID # 6419995
Pirenzepine	Tocris Bioscience	Cat # 1071; CAS # 29868–97-1; PubChem CID # 71405
Cevimeline	Tocris Bioscience	Cat # 3689; CAS # 107220–28-0; PubChem CID # 76965955
Xanomeline	Tocris Bioscience	Cat # 3569; CAS # 141064–23-5; PubChem CID # 18920248
VU0357017	Tocris Bioscience	Cat # 4295; CAS # 1135242-13–5; PubChem CID # 25010775
Retigabine	Toronto Research Chemicals	Cat # R189050; CAS # 150812–12-7; PubChem CID # 121892
XE991	Tocris Bioscience	Cat # 2000; CAS # 122955–13-9; PubChem CID # 45073462
VU0453595	Dr. Jeffery Conn, Vanderbilt University (Ghoshal et al., 2016)	N/A

Experimental Models: Organisms/Strains

REAGENT or RESOURCE	SOURCE	IDENTIFIER
Rhesus Macaque (Macaca Mulatta)	Yale University, Charles River, Coleston, University of Texas	N/A

Software and Algorithms

REAGENT or RESOURCE	SOURCE	IDENTIFIER
MATLAB v. 2018b	MathWorks	RRID:SCR_001622 https://www.mathworks.com/products/matlab/
GraphPad Prism	GraphPad Software	RRID:SCR_002798 https://www.graphpad.com/scientificsoftware/prism/
SPSS Statistics	IBM	RRID:SCR_002865 https://www.ibm.com/products/spss-statistics
Adobe Photoshop	Adobe	RRID:SCR_014199 https://www.adobe.com/products/photoshop.html
Adobe Illustrator	Adobe	RRID:SCR_010279 https://www.adobe.com/products/illustrator.html
3D Slicer	Slicer	RRID:SCR_005619 www.slicer.org